ISTANBUL TECHNICAL UNIVERSITY ★ ENERGY INSTITUTE

COMPUTATIONAL FLUID DYNAMICS ANALYSIS OF A THERMOCLINE THERMAL STORAGE UNIT FOR SOLAR THERMAL APPLICATIONS

M.Sc. THESIS

Azin ASADITAHERI

Energy Science and Technology Division

Energy Science and Technology Programme

Thesis Advisor: Dr. Lecturer Senem ŞENTÜRK LÜLE

DECEMBER 2018

ISTANBUL TECHNICAL UNIVERSITY ★ ENERGY INSTITUTE

COMPUTATIONAL FLUID DYNAMICS ANALYSIS OF A THERMOCLINE THERMAL STORAGE UNIT FOR SOLAR THERMAL APPLICATIONS

M.Sc. THESIS

Azin ASADITAHERI
(301171006)

Energy Science and Technology Division

Energy Science and Technology Programme

Thesis Advisor: Dr. Lecturer Senem ŞENTÜRK LÜLE

DECEMBER 2018

İSTANBUL TEKNİK ÜNİVERSİTESİ ★ ENERJİ ENSTİTÜSÜ

SOLAR TERMAL UYGULAMALAR İÇİN TERMOKLİN TERMAL DEPOLAMA ÜNİTESİ HESAPLAMALI AKIŞ DİNAMİĞİ ANALİZLERİ

YÜKSEK LİSANS TEZİ

Azin ASADITAHERI
(301171006)

Enerji Bilim ve Teknoloji Anabilim Dalı

Enerji Bilim ve Teknoloji Programı

Tez Danışmanı: Dr. Öğretim Üyesi Senem ŞENTÜRK LÜLE

ARALIK 2018

Azin Asadataheri, a M.Sc. student of ITU Institute of Energy student ID 301171006, successfully defended the thesis entitled "COMPUTATIONAL FLUID DYNAMICS ANALYSIS OF A THERMOCLINE THERMAL STORAGE UNIT FOR SOLAR THERMAL APPLICATIONS", which he prepared after fulfilling the requirements specified in the associated legislations, before the jury whose signatures are below.

Thesis Advisor :	**Dr. Lecturer Senem Şentürk Lüle** İstanbul Technical University	.....
Jury Members :	**Prof. Dr. Üner Çolak** İstanbul Technical University	.....
	Dr. Lecturer Barış Yılmaz Marmara University	.....

Date of Submission : 21 November 2018
Date of Defense : 13 December 2018

To my Family,

FOREWORD

I would like to express my deep appreciation and thanks to my advisor, Asst. Prof. Dr. Senem ŞENTÜRK LÜLE. This thesis was impossible without her warm guidance, support, and encouragement during the entire master study.

Special thanks to Prof.Dr. Üner ÇOLAK, for his positive and helpful guidance during the study.

December 2018

Azin ASADITAHERI
(Mechanical engineer)

TABLE OF CONTENTS

Page

ABBREVIATIONS

CFD **:** Computational Fluid Dynamics
HIK **:** Hacimsel Isı Kapasitesi
VHC **:** Volumetric Heat Capacity

SYMBOLS

α_f	: Thermal diffusivity, m^2s^{-1}
β	: Thermal expansion coefficient, K^{-1}
θ	: Dimensionless temperature
ρ	: Density, kg m^{-3}
ε	: Porosity
υ	: Kinematic viscosity, $m^2 s^{-1}$
g	: Gravitational acceleration, m s^{-2}
k	: Thermal conductivity, W $m^{-1}K^{-1}$
K	: Permeability of the porous medium
L	: Tank height, m
p	: Pressure, N m^{-2}
P	: Dimensionless pressure
Pr	: Prandtl number
Gr	: Grashof number
Rc	: Thermal conductivity ratio parameter
Re	: Reynolds number
C_p	: Specific Heat Capacity, J $kg^{-1}K^{-1}$
T	: Temperature, K
t	: Time, s
u	: Velocity components in x direction
v	: Velocity components in y direction
U	: Dimensionless velocity
x	: Cartesian coordinate, m
y	: Cartesian coordinate, m
X	: Dimensionless Cartesian, (x)
Y	: Dimensionless Cartesian, (y)
Da	: Darcy number

LIST OF TABLES

Page

LIST OF FIGURES

Page

COMPUTATIONAL FLUID DYNAMICS ANALYSIS OF A THERMOCLINE THERMAL STORAGE UNIT FOR SOLAR THERMAL APPLICATIONS

SUMMARY

World energy consumption increases every year therefore new power plants are necessary to meet the demand. Among many energy production systems, it is expected that share of renewable energy in total production is going to grow more than others due to environmental concerns and achievements at cost reduction. One of the renewable energy sources is sun and a solar power plant captures the sunlight and converts it into electricity.

There are several ways to harvest the sun's energy. Photovoltaic systems use panels to directly convert sunlight into electricity whereas solar concentrating systems use mirrors to reflect and focus sunlight on heat collecting component of the system where heat is transferred to a fluid which is used to generate steam to turn the turbine and generator to generate electricity as in thermal or nuclear power plants.

Concentrating solar systems has various configurations such as parabolic through, parabolic dish, and central tower. In parabolic through systems, there are reflector mirrors and receiver tubes which are located at focal axis of mirrors. Sun rays are reflected to the receiver tube and heat is transferred to fluid inside the tube. This fluid is then used with conventional steam generator to produce electricity. In parabolic dish systems, sun rays are reflected to the center of the dish where receiver is placed. The heat machine on the receiver that moves with the dish uses Stirling or Brighton cycle for power conversion. On the other hand, in central tower systems sun rays are reflected to the receiver at the top of the tower by mirrors around the tower. Conventional steam generator is used for electricity generation.

The electricity form solar power plant is categorized as intermittent electricity due to the fact that it cannot be continuously available. As a result, fluctuating demand of electricity cannot be met therefore solar power plants are considered non-dispatchable. On the other hand, it is possible to constrain intermittency either with direct electricity storage for photovoltaic systems or with thermal energy storage for concentrating systems. In thermal energy storage, some of the heat form the receiver is stored in the storage unit for later use. Since storing thermal energy is cheaper than storing electricity itself, the focus is on development of thermal energy storage systems. Efficient and cost-effective storage is an important tool to increase the share of solar energy in the electricity market.

There are two options available for thermal energy storage: two-tank storage and single-tank thermocline storage. In two tank storage, during charge cycle, fluid from cold tank passes through a heat exchanger if system is indirect or collector field if system is direct to hot tank and during discharge cycle fluid moves back from hot tank to cold tank after passing through steam generator. In single-tank thermocline storage, there is a filler material in the tank as energy storage medium. During charge cycle, cold fluid moves from the bottom of the tank towards the heat exchanger and returns

to the tank from the top as hot fluid and during discharge cycle, hot fluid moves from the top of the tank towards heat exchanger and returns the tank from the bottom as cold fluid. Since part of fluid in the two-tank storage system is replaced with a filler material which is usually cheap, single-tank thermocline storage offers cost-effective energy storage.

In the scope of this thesis, single-tank thermocline thermal energy storage discharge cycle analysis with computational fluid dynamics (CFD) was considered because the literature review showed that focus is generally on the properties of storage tanks and sensitivity analysis of storage tanks with correlation and formulation.

Therefore, with the CFD analysis stream-lines and velocity and temperature distribution in the thermocline tank together with the effects of porosity, sphericity and type of fluid on discharge process were investigated. Seven different heat transfer fluids having various specific heat capacity values were considered. In order to see the effect of porosity in the tank, three porosity values were selected. The effect of the filler material geometry was included by using four different sphericity values.

First of all, the geometry of the thermocline tank was determined with literature review. Then, the mathematical model to perform simulations were defined. The governing equations of continuity, time dependent momentum, and time dependent energy are included in openFOAM CFD code. Governing equations include not only effective conductivity and Forchheimer-Brinkman approximation but also Bouyssinisq approximation. The grid independence study which guarantees the independence of results from the mesh size was performed. Later, base input of the CFD code which includes the model of the reference thermocline tank from literature was validated by comparing simulation results with experimental data. Finally, simulations were performed with selected heat transfer fluids for different operating conditions i.e., porosity and sphericity and their effect on thermocline storage tank energy deposition and energy generation was discussed.

The simulation results showed that when the fluid has high value of volumetric heat capacity (VHC), the initial energy stored in the tank increases. In addition, if VHC value of the fluid is lower than the value for the filler material, initial energy stored in the tank is mainly stored in the filler material. The percentage of the stored energy in the solid drops as low as 50% if the fluid has high VHC and tank has high porosity. Furthermore, for fluids with high values of VHC, when the porosity of the thermocline tank increases, the amount of energy remained in the tank during discharge cycle increases. On the other hand, fluids with low values of VHC, higher porosity value results in lower remaining energy in the tank. On the other hand, temperature profiles and streamlines of the 6 hours of discharge showed that for low values of porosity, higher sphericity value prevents mixing of hot and cold fluid and results in better discharge performance. It is clear from the simulations that discharge behaviour of the storage tank mainly depends on the relation between the VHC of fluid and solid filler material, high value of sphericity provides positive effect on discharge performance as long as porosity is low, and porosity value selection must include fluid and solid VHC values.

Future studies can be done to increase the efficiency of the tank by improving stream-line pattern. It is known that when the stream-lines are uniform, mixing of hot and cold fluid reduces and efficiency of the tank increases. It is possible to reach this goal by making modifications inside the tank such as creating lanes for the flow. Another possible area of study can be usage of nano-fluids as heat transfer medium. These

studies can be performed efficiently with computational fluid dynamics simulations which use the experimentally verified mathematical model developed in this study.

SOLAR TERMAL UYGULAMALAR İÇİN TERMOKLİN TERMAL DEPOLAMA ÜNİTESİ HESAPLAMALI AKIŞ DİNAMİĞİ ANALİZLERİ

ÖZET

Enerji tüketimi her yıl artmaktadır ve bu nedenle talebi karşılayacak yeni güç santrallerine ihtiyaç duyulmaktadır. Tüm enerji üretim sistemleri arasında yenilenebilir enerjinin payının çevresel kaygılar ve maliyetlerin azaltılmasındaki başarılar nedeniyle artması beklenmektedir. Yenilenebilir enerji kaynaklarından biri güneştir ve güneş santralleri güneş enerjisini elektriğe dönüştüren sistemlerdir.

Güneş enerjisini kullanmanın çeşitli yolları vardır. Fotovoltaik paneller ile güneş enerjisini direkt olarak elektriğe çevirmek mümkünken, yoğunlaştırılmış sitemlerde güneş ışığının belirli bir noktaya odaklanarak yansıtılması ile enerjinin ısı taşıyıcı bir akışkana iletilip nükleer ya da termik santrallerdeki gibi buhar çevrimi yolu ile elektrik üretilmesi de mümkündür.

Yoğunlaştırılmış güneş sistemleri parabolik oluk, parabolik çanak ve merkezi kule gibi değişik düzenlerde olabilir. Parabolik oluk sistemlerinde odak noktalarının ekseninde içinde akışkan dolaşan alıcı tüplerin bulunduğu yansıtıcı aynalar mevcuttur. Aynaya ulaşan güneş ışınları yansıyarak alıcı tüplerin içindeki akışkanı ısıtırlar. Bu akışkan daha sonra konvansiyonel buhar üreteçleri ile elektrik üretiminde kullanılır. Parabolik çanak sistemlerinde ise çanak eksenine paralel olarak gelen güneş ışınları aynalar tarafından çanak merkezine yansıtılarak buradaki alıcıya ulaştırılır. Toplanan ısı çanak ile birlikte hareket eden alıcıdaki ısı makinası ile Stirling veya Brighton çevrimi için kullanılır. Diğer bir taraftan, merkezi kule sistemlerinde pek çok yansıtıcı ayna güneş ışınlarını merkezi kulenin tepesinde bulunan alıcıya iletirler. Alıcıda ısınan akışkan konvansiyonel buhar üreteçlerinde elektrik üretimi için kullanılır.

Güneş santralleri elektriği sürekli olarak üretilemediği için bu elektrik kesintili elektrik olarak kategorize edilir. Bu nedenle, elektrik talebindeki dalgalanmalar karşılanamaz. Diğer bir taraftan, kesintili elektrik üretimi fotovoltaik sistemlerde elektriğin direkt depolanması, yoğunlaştırılmış sistemlerde ise termal enerji depolama ile kısmen engellenebilir. Termal enerji depolamada alıcıdan gelen ısının bir kısmı daha sonra kullanılmak üzere depolanır. Elektriği depolamak termal enerjiyi depolamaktan pahalı olduğu için termal enerji depolama sistemlerine odaklanılmıştır. Verimli ve uygun maliyetli termal enerji depolama güneş enerjisinin elektrik üretim piyasasındaki yerinin arttırılmasında önemli bir unsurdur.

Termal enerji depolamada iki yöntem mevcuttur: iki-tank depolama ve tek-tank termoklin depolama. İki-tank depolamada, dolum çevriminde soğuk tanktaki akışkan endirekt sistemlerde ısı değiştiriciden direkt sistemlerde ise kollektör alanından geçerek sıcak tanka, boşaltım çevriminde ise sıcak tanktaki akışkan buhar üretecinden geçtikten sonra soğuk tanka geri döner. Tek-tank termoklin depolamada ise bir tank vardır ve tankın içi katı bir dolgu malzemesi ile doludur. Bu kısım asıl termal depolama ortamıdır. Dolum çevriminde, soğuk akışkan tankın alt kısmından çekilerek ısı

değiştiriciye yönlendirilir ve ısınmış olarak tankın üst kısmından tanka geri döner. Boşaltım çevriminde ise sıcak akışkan tankın üst kısmından çekilerek ısı değiştiricisine gidip ısısını kaybederek tanka soğumuş olarak alt kısımdan giriş yapar. İki-tank depolamada kullanılan ve genellikle pahalı olan akışkan nispeten daha ucuz dolgu malzemesi ile değiştirildiğinden, tek-tank termoklin depolama daha ekonomik bir enerji depolama sağlamaktadır.

Bu tez kapsamında, hesaplamalı akış dinamiği ile tek-tank termoklin termal enerji depolama sistemi boşaltım döngüsü analiz edilmiştir. Çalışmanın temelini literatürde yapılan çalışmaların daha çok tank özellikleri üzerine ve hassasiyet analizlerinin ise genellikle korelasyonlar ile yapılması oluşturmaktadır.

Bu nedenle, hesaplamalı akış dinamiği benzeşimleri ile tank içindeki akış hatları ile sıcaklık ve hız dağılımlarını gözlemek mümkündür. Ayrıca boşluk oranı, küresellik faktörü ve farklı akışkanların boşaltım çevrimi üzerindeki etkilerini de incelemek mümkündür. Bu çalışmada yedi akışkan dikkate alınmıştır. Ayrıca, üç farklı boşluk oranı ve dolgu malzemesinin etkilerinin incelenmesi için de dört farklı küresellik faktörü kullanılmıştır.

Çalışmada ilk olarak modellenecek termoklin tank literatür taraması sonucu belirlenmiştir. Ardından, benzeşimlerde kullanılacak matematik model oluşturulmuştur. Süreklilik, zamana bağlı momentum ve zamana bağlı enerji korunum denklemleri hesaplamalı akış dinamiği kodu openFOAM'a dâhil edilmiştir. Korunum denklemleri sadece efektif ısıl iletkenlik ve Forchheimer-Brinkman yaklaşımlarını değil Bouyssinisq yaklaşımını da içermektedir. Daha sonra, benzeşim sonuçlarının geometri için oluşturulan kafes sisteminden bağımsız olması sağlanmıştır. Ardından, referans tank için oluşturulan temel girdi verisi benzeşim sonuçları deneysel sonuçlar ile karşılaştırılmış böylece geometrik ve matematik modellerin düzgün bir biçimde oluşturulduğu doğrulanmıştır. Son olarak, seçilen akışkanların ve çalışma koşullarının (değişik boşluk oranları ve küresellik faktörleri) boşaltım çevrimi üzerindeki etkilerini araştırmak üzere pek çok benzeşim yapılmış ve sonuçlar tartışılmıştır.

Benzeşim sonuçlarına göre, yüksek hacimsel ısı kapasitesine (HIK) sahip akışkanlar tank içinde daha fazla ilk enerji depolanmasını sağlamaktadırlar. Bununla birlikte, akışkanın HIK değeri katı dolgu maddesinin HIK değerinden az ise depolanan enerji çoğunlukla katı dolgu maddesinde bulunmaktadır. Katıda depolanan enerji HIK değeri ve boşluk oranı arttıkça %50 seviyelerine kadar düşmektedir. Gözlenen bir diğer olgu da yüksek HIK değerine sahip akışkanlar için boşluk oranı arttıkça boşaltım sonunda tankta kalan enerjinin artmasıdır. Bu durum düşük HIK değerine sahip akışkanlarda ise tam tersidir. Ancak, 6 saatlik boşaltımın zamanla tank içinde neden olduğu sıcaklık dağılımına bakıldığında düşük boşluk oranı için küresellik faktörünün artması sıcak ve soğuk sıvının karışmasını engellemekte ve tank performansını arttırmaktadır. Simülasyon sonuçlarına göre, boşaltım döngüsünün ısıl davranışı çoğunlukla akışkan ve katı dolgu malzemelerinin HIK değerleri arasındaki ilişkiye bağlıdır, düşük boşluk oranı ile yüksek küresellik faktörünün kullanılması tank performansını olumlu yönde etkilemektedir ve tank için belirlenecek olan boşluk oranı ve küresellik faktöründe katı dolgu maddesinin ve akışkanın hacimsel ısı kapasiteleri dikkate alınmalıdır.

Bu çalışmanın devamında tank verimini arttırmak için akış hatları üzerinde iyileştirme çalışmaları yapılabilir. Bilindiği üzere akış hatları düzgün olduğunda, soğuk ve sıcak akışkanın karışması azalacak ve tank verimi artacaktır. Bu amaçla tank içinde akış şeritleri oluşturmak gibi bir takım tasarım değişiklikleri yapılabilir. Bir başka muhtemel çalışma alanı da nano-akışkanların ısı transfer sıvısı olarak kullanılması

olabilir. Deneysel veriler ile doğrulanan, tezde oluşturulan matematiksel modeli kullanan hesaplamalı akış dinamiği benzeşimleri ile bu tür çalışmalar hızlı bir şekilde yapılabilir.

1. INTRODUCTION

As the world energy consumption increases, it became vital to construct new power plants. When the environmental issues were taken into consideration, renewable power attracts more attention than any other means of generating electricity. Solar power is a strong collaborator to electricity production especially with concentrating solar systems. Brenna et al. (2008) described solar concentrating systems as "when solar irradiation comes into the optical collector plate, they are combined and become condensed solar radiation and then moved to the receiver. The receiver then absorbs the thermal energy of the solar radiation, and then the thermal energy absorbed is transferred to turbine-generator system by the operating fluid. This will lead to electricity generation". Concentrating solar systems has various configurations such as parabolic through, parabolic dish, and central tower.

Parabolic through type, consists of mirrors and receiver tubes that are at the focus line of the mirrors (Khan et al., 2016). When the sun rays hit the mirror (Figure 1.1), the mirror reflects the sun rays onto the black-coated metallic tube at the focus line. The fluid in the tube absorbs the heat and transfers it to the heat exchanger. The reflector is used to track the sun during the daylight. Generated steam is used rotate the turbine and generator to produce electricity (Mills, 2004).

Figure 1.1 : Parabolic trough system (Khan et al., 2016).

The parabolic dish type solar system operates by focusing the sun rays on a focal point by directing all sun rays parallel to the axis of the parabola to its center. The receiver is located at the focal point (Figure 1.2). The heat machine on the receiver uses Stirling or Brighton cycle for power conversion.

Figure 1.2 : Parabolic dish system (Siva et al., 2012).

The solar tower is also known as a heliostat collector or central receiver-based solar collector. The solar beams that hit the heliostats are directed to the central receiver at the top of the tower which is located in the middle of the system. Therefore, tower can receive all directed sun rays reflected by the heliostat mirrors. The mirrors used in this system are slightly concave, and the maximum amount of energy is directed to the steam generator to produce steam at high pressure and temperature **(**Kaushika et al., 2000).

Figure 1.3 : Tower system (Kaushika et al., 2000).

For all the systems described above energy storage can provide energy efficiency. Efficient and cost-effective storage is an important tool to increase the share of solar

energy in the electricity market. The schematic diagram of concentrating power plant with energy storage is shown in Figure 1.4.

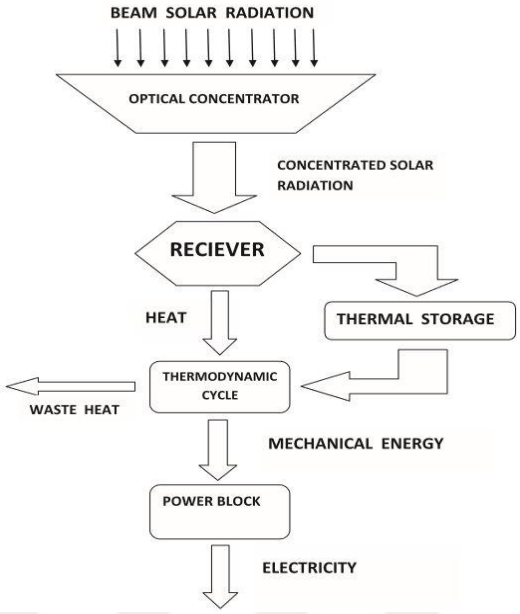

Figure 1.4 : Principle diagram of concentrated solar power plant with energy storage (Brenna et al., 2008).

As seen in Figure 1.4, some of the heat form the receiver is stored in the storage unit for later use. This unit could be a two-tank or single-tank thermocline storage. In two-tank system, cold and hot fluid is stored in different tanks. In two-tank storage, during charge cycle, fluid from cold tank passes through a heat exchanger if system is indirect (Figure 1.5) or collector field if system is direct (Figure 1.6) to hot tank and during charge cycle fluid moves back from hot tank to cold tank after passing through steam generator.

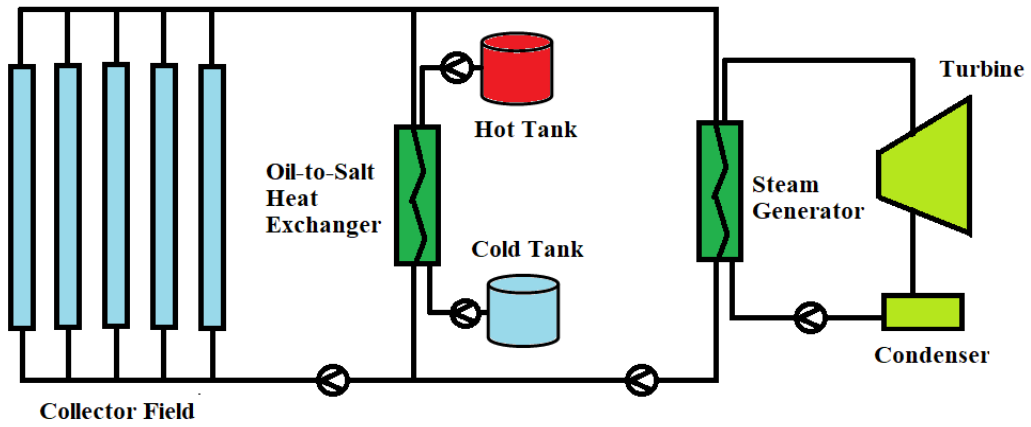

Figure 1.5 : Indirect, two-tank thermal energy storage schematic (Brosseau et al., 2004).

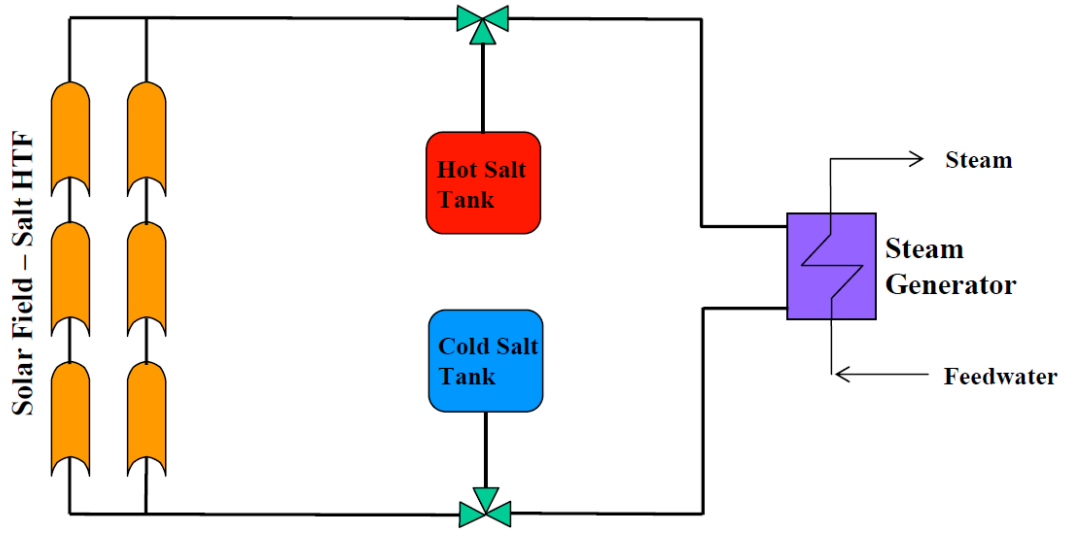

Figure 1.6 : Direct, two-tank thermal energy storage schematic (Brosseau et al., 2004).

In single-tank thermocline storage, the tank is filled with a filler material which is the main thermal storage medium. During the charge cycle, cold fluid moves from the bottom of the tank towards the heat exchanger and returns to the tank from the top as hot fluid and during the discharge cycle, hot fluid moves from the top of the tank towards heat exchanger and returns the tank from the bottom as cold fluid (Figure 1.7). Since part of fluid in the two-tank storage system is replaced with a filler material which is usually less expensive, single-tank thermocline storage offers cost-effective energy storage.

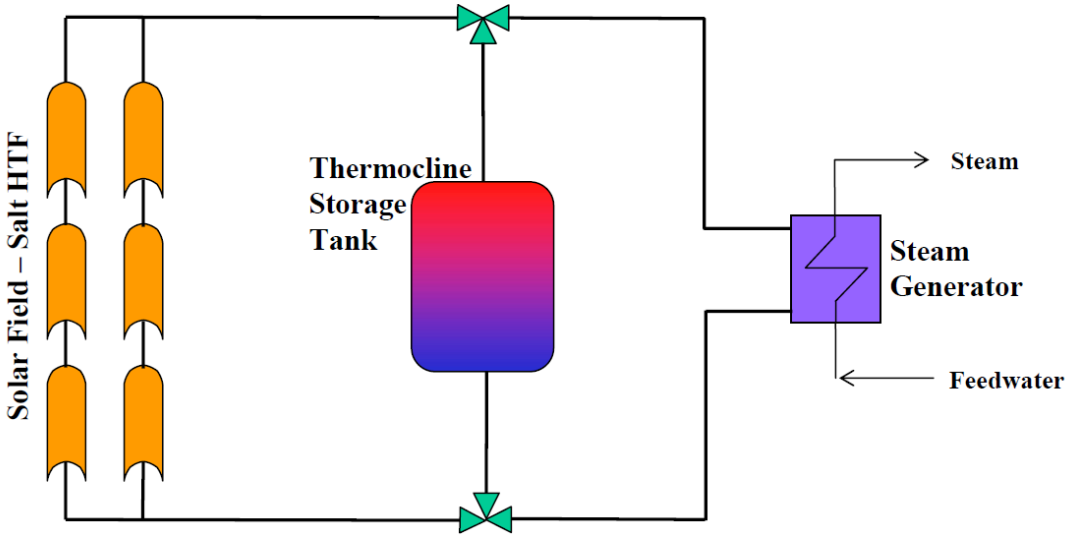

Figure 1.7 : Direct single-tank thermocline storage system schematic (Brosseau et al., 2004).

2. LITERATURE REVIEW

According to Gil et al. (2010), the production of concentrated thermal energy has become a highly attractive integrated energy production system among all the various renewable alternatives because it has a better potential for dispatchability. Since dispatchability is eventually connected to efficiency, cost-effective thermal storage is the key component. Only a few plants in the world have tested high-energy energy storage systems.

The governing equations to simulate thermal storage were obtained by using a new perspective on the numerical method by Brosseau et al (2005). The governing equations were reduced to dimensionless forms, which allows the universal use of the solution. Hyperbolic type dimensional equations were numerically solved. Proposed numerical method solves numerical problems explicitly, implicitly, and limits the infinite-NTU method and offers a direct solution to differential equations (without the required duplicate calculation) and completely eliminates any computational overhead. An independent network solution was achieved in a small number of nodes and it was proved that the method is fast, efficient, and accurate. In addition, another model was developed to enable the analysis of several types of heat-insulating heat systems at the time they are connected to a network. It was shown that this model also has flexibility to allow different connection designs for the charge/discharge process of tank.

Bonanos at al. (2016) proposed single-tank thermocline thermal energy storage as an efficient alternative at competitive cost to the traditional two-tank storage. Therefore, sensitivity analysis was performed to determine the parameters that have the greatest impact on efficiency. The results showed that the reservoir height, together with the thermo-physical properties of the solid filler material, has the highest effect on reservoir efficiency with fluid properties has secondary effect.

HITEC Melt Salt as fluid and quartzite rocks as filler were deployed by Yang et al. (2010) to model transfer of heat between two phases by using interstitial heat transfer coefficient to investigate temperature profiles and discharge efficiency of solar thermal

systems. The mass and momentum equations were calculated on average, with the extension of the Brinkman-Forchheimer command to the Darcy law which used for the porous resistance model of the environment. The governing equations were solved using a finite approach. It was concluded that efficiency of the discharge improved when Reynolds's number is small and reservoir height is high. In addition, size of the filler particles greatly affected the amount of internal heat transfer and thus the discharge efficiency.

Xu et al. (2012) indicated that the effective heat transfer coefficient with distributed capacitance method can be used to simulate thermal storage. Four typical structures for solid thermal storage materials were considered. It was shown that effective heat transfer coefficient increased the reliability of the distributed capacitance method.

In their studies, Bayon et al. (2013) ignored the thermal losses and expressed the heat transfer equation in terms of endless coordinates to simplify the process of solving and obtaining overall results in terms of performance parameters of thermocline in storage tanks. The simulation with the CIEMAT1D1SF model showed that the performance of the thermocouple reservoir strongly depends on the height of the reservoir and the fluid velocity. Therefore, it was indicated that small prototype vessels do not behave same as big thermocouple reservoir meaning similarity analysis cannot be applied directly.

Experimental and numerical tests of thermocline thermal tank with molten-salt which is an inexpensive option to store thermal energy in solar energy systems were performed by Flueckiger et al. (2013) to identify key issues related to the design and operation of the tank. The results showed that performance of the tank discharge was improved by increasing the height of the tank and by reducing the diameter of the inner filler due to increased thermal uniformity and continuous output of molten salt with high thermal quality. In addition, it was concluded that reduction of the flow rate of the fluid in a well-insulated (adiabatic) tank reduced the temperature range of the area and increases the efficiency.

To provide an effective tool for tank design, Li et al. (2011) used the governing equations for fluid-free heat transfer for liquid and solid filler materials and examined all scenarios of the charge and energy process. At the end, power saving curves considering four important parameters i.e. the dimensions of the storage tank, the

properties of the liquid, the properties of filler materials, and the operating conditions were achieved. The curves then generalized as charts and served for the purpose of designing and calibrating the dimensions of thermal storage tanks and operating conditions without making complex computations or simulations.

Zurigat et al. (1991) investigates the effect of input geometry on the achievable degree in thermal energy storage of thermocline. Analysis showed that input geometry begins to affect the thermal classification in a thermocline thermal storage tank when Richardson number is below 3.6.

A new single-phase perturbation model involving a series of expansion solution to disruption model proposed by Votyakov et al. (2014) to investigate the behavior of packed thermocline thermal energy storage tanks. It was shown that it is an improvement over the current models since it more accurately takes the effect of diffusion into account. In addition, it provides a direct comparison with the two-phase and one-phase models.

One of the experimental studies in the literature about the investigation of effects of a porous manifold on the construction and maintenance of a thermal classification in a liquid storage tank was performed by Brown et al. (2011). 315 liters, height to radius ratio 4 tank with porous manifold of nylon plate in tube was used. The classification was observed at Richardson's number below 0.615. Flow pattern confirmed the effectiveness of porous manifolds in enhancement and maintaining a stable thermal classification due to their capability of reducing the shear-induced mixing between fluids with different temperatures.

Another experimental study that investigate the thermal storage system was performed by Forsberg et al. (2007). 6.5 MW experimental setup to observe thermocline production consisted of a packed bed of stones as filler material and air at high temperature as heat transfer fluid. In addition, a numerical and dynamic heat transfer model that is used to calculate thermal properties and physical variables in the range of 20-650 ^{o}C was presented. The results confirmed by experimental results.

In the work presented by Chang at al. (2014), a two-dimensional model of thermocline thermal storage system was designed to understand the effects of the properties of the storage media (both solid and liquid materials) and of the boundary conditions of the input flow on thermal performance of the storage system. The results show that the

thermocline thickness increases by use of solar salts as heat transfer fluid and Cofalit as a solid material. In addition, non-uniformity in the flow of the inlet stream just increases the mixing fluid and the expansion of the heat in a substantial path, which results in the loss of the thermodynamic access of stored energy. The thickness of the thermocline increases with the inappropriateness of the boundary conditions of input velocity. Therefore, the lower non-uniformity of the inlet flow is better, although it may result larger volatility at the average output temperature. It is better for the thermocline storage tank to have smaller input mass flow.

3. MATHEMATICAL MODELING

Since this study includes numerical investigation of the heat transfer, the flow pattern, and the total thermal energy (time dependent) of a thermal storage in a cylindrical tank, the mathematical model includes porous region parameters. To obtain the results, the governing equations of continuity, time dependent momentum, and time dependent energy must be solved. Governing equations include not only effective conductivity and Forchheimer-Brinkman approximation but also Bouyssinisq approximation. As validated by Taghizadeh et al. (2018), the temperature difference between the solid and liquid in the porous region is ignored according to local thermal equilibrium model.

Based on assumptions, the non-dimensional variables are defined as below:

$$X = \frac{x}{L}, Y = \frac{y}{L}, U = \frac{u}{U_0}, V = \frac{v}{U_0}, \theta = \frac{T - T_c}{T_h - T_c}, P = \frac{p}{\rho U_0{}^2}, \tau = \frac{t\nu}{d^2} \tag{3.1}$$

$$k_{eff} = \xi k_f + (1-\xi) k_p, R_c = \frac{k_{eff}}{k_f} \tag{3.2}$$

$$\mathrm{Re} = \frac{U_0 L}{\upsilon}, Gr = \frac{g\beta(T_h - T_c)L^3}{\upsilon^2}, \mathrm{Pr} = \frac{\upsilon}{\alpha_f}, Da = \frac{K}{L^2} \tag{3.3}$$

where X and Y are infinitely distant and they are measured horizontally and vertically. U and V are components of dimensionless velocity in the direction of X and Y. θ represents the dimensionless temperature. P is dimensionless pressure; k is the average permeability; Da, Re, and Pr represent Darcy number, Reynolds and Prandtl numbers. ε is the mean effective porosity and R_c is the thermal conductivity ratio. Taking into account above assumptions and dimensionless variables, the governing equations in the normalized state to represent the flow phenomenon in the clear liquid region are given in Equation 3.4 to 3.7.

$$\frac{\partial U}{\partial X}+\frac{\partial V}{\partial Y}=0 \tag{3.4}$$

$$U\frac{\partial U}{\partial X}+V\frac{\partial U}{\partial Y}=-\frac{\partial P}{\partial X}+\frac{1}{\mathrm{Re}}\left(\frac{\partial^2 U}{\partial X^2}+\frac{\partial^2 U}{\partial Y^2}\right) \tag{3.5}$$

$$U\frac{\partial U}{\partial X}+V\frac{\partial U}{\partial Y}=-\frac{\partial P}{\partial X}+\frac{1}{\mathrm{Re}}\left(\frac{\partial^2 V}{\partial X^2}+\frac{\partial^2 V}{\partial Y^2}\right)+\frac{Gr}{\mathrm{Re}^2}\theta \tag{3.6}$$

$$U\frac{\partial \theta}{\partial X}+V\frac{\partial \theta}{\partial Y}=\frac{1}{\mathrm{Pr}\,\mathrm{Re}}\left(\frac{\partial^2 \theta}{\partial X^2}+\frac{\partial^2 \theta}{\partial Y^2}\right) \tag{3.7}$$

At the same time, the general form of the governing equation in a porous region is based on the mean Navier-Stokes equations on the representative initial volume and is presented using the Darcy-Forchheimer Brinkman model (Taghizadeh et al. 2018) and given in Equations 3.8 to 3.11.

$$\frac{\partial U}{\partial X}+\frac{\partial V}{\partial Y}=0 \tag{3.8}$$

$$\frac{1}{\xi^2}\left(U\frac{\partial U}{\partial X}+V\frac{\partial U}{\partial Y}\right)=-\frac{\partial P}{\partial X}+\frac{1}{\xi\,\mathrm{Re}}\left(\frac{\partial^2 U}{\partial X^2}+\frac{\partial^2 U}{\partial Y^2}\right)-\frac{1}{\mathrm{Re}\,Da}U \tag{3.9}$$

$$\frac{1}{\xi^2}\left(U\frac{\partial V}{\partial X}+V\frac{\partial V}{\partial Y}\right)=-\frac{\partial P}{\partial X}+\frac{1}{\xi\,\mathrm{Re}}\left(\frac{\partial^2 V}{\partial X^2}+\frac{\partial^2 V}{\partial Y^2}\right)+\frac{Gr}{\mathrm{Re}^2}\theta-\frac{1}{\mathrm{Re}\,Da}V-\frac{F}{\sqrt{Da}}V\sqrt{U^2+V^2} \tag{3.10}$$

$$U\frac{\partial \theta}{\partial X}+V\frac{\partial \theta}{\partial Y}=\frac{R_c}{\mathrm{Pr}\,\mathrm{Re}}\left(\frac{\partial^2 \theta}{\partial X^2}+\frac{\partial^2 \theta}{\partial Y^2}\right) \tag{3.11}$$

Here F is the inertia Forchheimer coefficient which can be mathematically expressed as in Equation 3.12.

$$F = \frac{1.75}{\sqrt{150\xi^2}} \tag{3.12}$$

Since porous field has important effect on model conductivity, based on Forchheimer Brinkman model, an effective conductivity has influence on the system heat transfer.

Permeability of system is an important parameter which depends on porosity and particle diameter and sphericity. Porosity is defined as fraction of void volume to total volume. Sphericity is a precise measure of the shape of an object and always varies between zero and one ($0<\tau\leq1$). The permeability formula known as Carmen – Kozeny Equation is presented in Equation 3.13.

$$K = \frac{\xi {d_p}^2}{8s} \tag{3.13}$$

To insert permeability effect in governing equations by using Darcy-Forchheimer approximation in computational fluids dynamics code used for simulations (openFOAM), two parameters must be determined; viscous and inertial resistance b and f. Equations for viscous resistance b and inertial resistance f are given in Equation 3.14 (Jones, 2001).

$$b = \frac{1}{K},\ f = 4.9659\times10^{-8}\times K^{-1.55} \tag{3.14}$$

It should be noted that depending on effective conductivity, Prandtl and diffusion coefficient has to be corrected and effective value of them must be calculated.

4. COMPUTATIONAL FLUID DYNAMICS STUDIES

Open source, free software openFOAM was used to perform computational fluid dynamics (CFD) analysis of the storage tank. Stream-lines and velocity and temperature distributions of the discharge process of different heat transfer fluids for different operating conditions such as porosity and sphericity were compared to understand their effect on storage tank performance.

4.1 General Description of the Problem

In order to perform CFD simulations, a thermocline tank (Figure 4.1) described in detail in (Yang et al., 2010), (Bonanos et al., 2016), and (Pracheco et al., 2001) was used in this study. Parameter *h* represents the height of the tank where filler and fluid are positioned together and *h′* represents area in the tank where just fluid exists. Parameter *d* is the diameter of tank and *d′* is the diameter of inlet and outlet pipe.

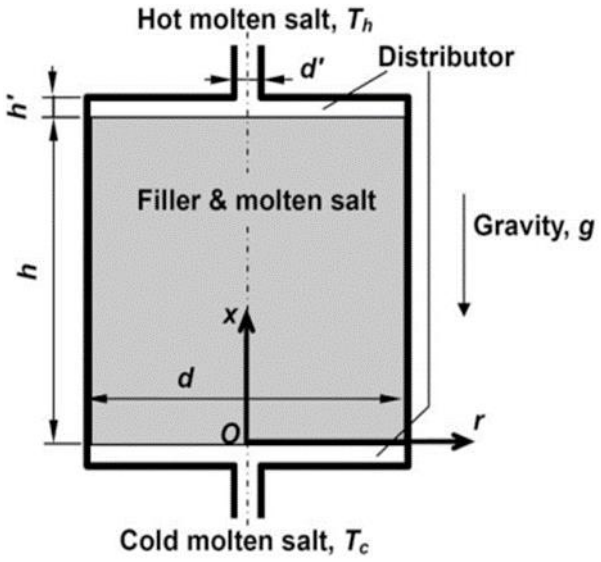

Figure 4.1 : Tank geometry used in this study (Yang et al., 2010).

The dimensionless form of parameters (Equation 4.1) and their values used for the simulations are as follows:

$$H = \frac{h}{d_p}, H' = \frac{h'}{d_p}, D = \frac{d}{d_p}, D' = \frac{d'}{d_p} \quad (4.1)$$

where: H=67, H′=1.1, D=33, D′=3.3, and d_s=0.1.

In this study, inlet of tank located at bottom whereas outlet is located at top of the tank therefore during discharge cycle, cold fluid enters the tank from the bottom and hot fluid exits the tank from the top. Since tank design has symmetry on cylindrical angle, 2 dimensional simulations were considered.

The corresponding boundary conditions in dimensionless form used in this study are as follows:

1) The tank has just one inlet and one outlet.
2) Inlet and outlet flows are calculated based on *Re* number.
3) Inlet flow temperature considered to be constant at low temperature.
4) Walls of the tank have zero gradient boundary condition (heat losses are zero).

At the interface of two fluid and porous medium zones the following boundary conditions are applied:

1) Effective viscosity equals to fluid viscosity $\mu_{eff} = \mu_f$ (Taghizadeh et al. 2018).
2) Porous section has same temperature as fluid section due to small *Re* number.

In order to solve governing equations described in previous section with corresponding boundary conditions, governing equations were constructed based on PIMLPE. To interpret the control terms in the governing equations, the predicted scheme was used together with second-order planning which interprets the terms. In order to obtain converged solution, the optimal value of the relaxation factor was chosen based on computational experiments. The convergence criterion was set for relative residue of all variables and all components of speed and temperature as 10^{-6}.

4.2 Grid Independence Study

For computational fluid dynamics simulations, it is important to ensure grid independence of the results. In general, a course mesh simulation result and a fine mesh simulation result of the same problem is not the same; the latter being better. Grid independence study provides the solution not to vary in large even when mesh is

refined further. Therefore, prior to comprehensive simulations, mesh sensitivity analysis was performed by generating six non-uniform meshes shown in Figure 4.2.

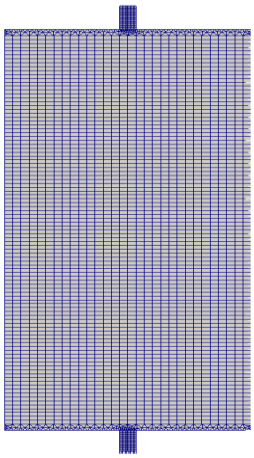

(a) 100 vertical-30 horizontal
3000 nodes

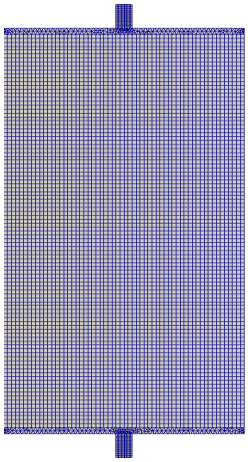

(b) 100 vertical-60 horizontal
6000 nodes

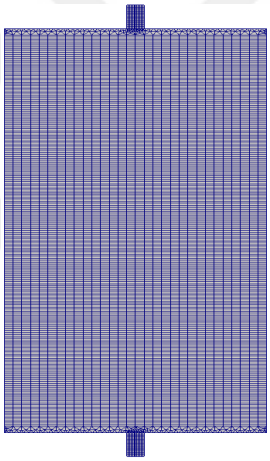

(c) 200 vertical-30 horizontal
6000 nodes

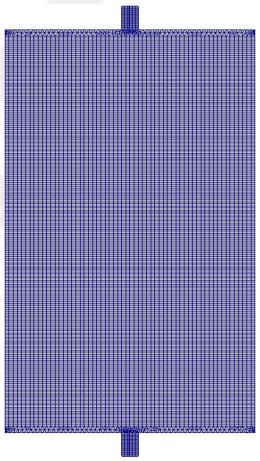

(d) 200 vertical-60 horizontal
12000 nodes

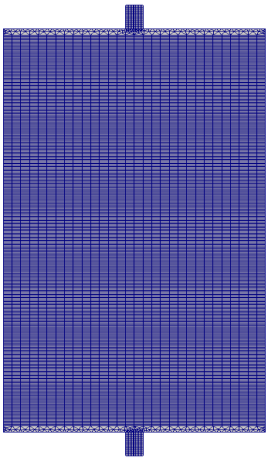

(e) 400 vertical-30 horizontal
12000 nodes

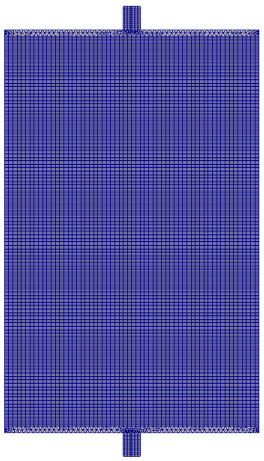

(f) 400 vertical-60 horizontal
24000 nodes

Figure 4.2 : Different meshes generated for grid independence study.

For the grid independence study, these six different meshes were used to simulate the experiment described in Pacheco et al. (2001). In the experiments, HITEC Salt is the heat transfer fluid and quartzite rock is the filler material which's parameters were taken from Yang et al. (2010). For simulation purposes parameters were defined as *Re* number being 220, *Pr* number being 13.4, *Gr* number being 9.59×10^7 and finally *Da* number being 0.01. Table 4.1 shows variation of simulated average temperature in the middle of the tank according to different meshes. It is seen that the difference between the results of the mesh having 3000 and 24000 nodes is less than 0.09%.

Table 4.1 : Average temperature at middle of the tank for different meshes.

Mesh Size	100^a-30^b	100^a-60^b	200^a-30^b	200^a-60^b	400^a-30^b	400^a-60^b
Average temperature at the middle of the tank, (K)	583.42	583.55	583.06	583.11	582.97	582.95

[a]number of vertical nodes, [b]number of horizontal nodes.

The axial temperature at midline of the tank from six simulations were also compared with the experimental data given in Yang et al. (2010) at 2222 second of the experiment and presented in Figure 4.3.

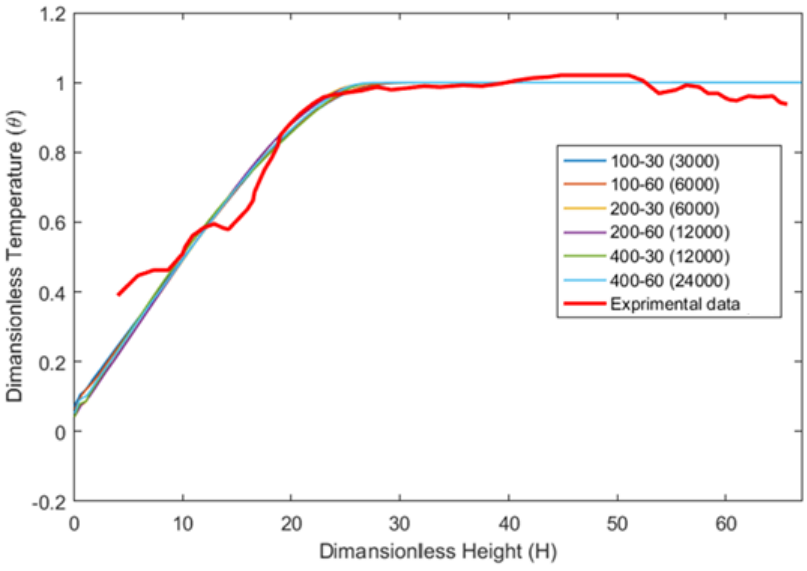

Figure 4.3 : Comparison of dimensionless axial temperature at midline with experimental data of Pacheco et al. (2001).

Considering the difference between the results and computational time, the simulations continued with 100 vertical-60 horizontal totaling 6000 nodes mesh configuration.

4.3 Validation of the CFD Model

To validate the numerical model generated with openFOAM for simulations, heat transfer problem in the tank was investigated. The results of the simulation are compared with experimental and computational results in the literature. The discharge process was simulated where fluid inlet is located at the bottom of the tank and output is located at the top of the tank. The simulations were performed to have similar time scale with experiments.

Figure 4.4 shows the variation of dimensionless temperature with dimensionless height for various dimensionless time values. The numerical model used shows good agreement with experimental data of Paroncini et al. (2001) and numerical studies of (Yang et al., 2010 and Bonanos et al., 2016).

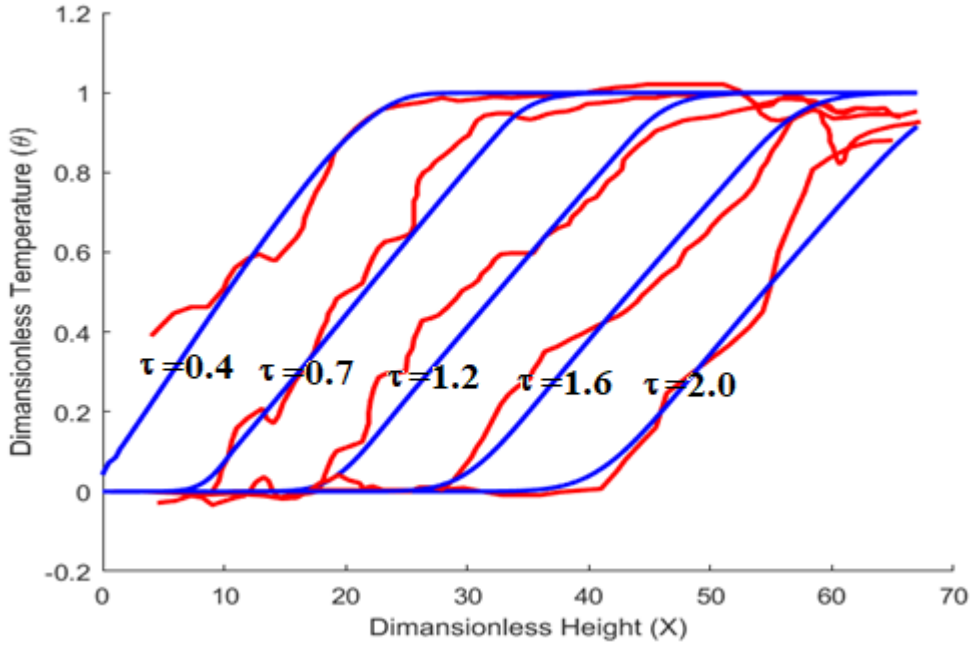

Figure 4.4 : Variation of dimensionless temperature with dimensionless height during discharge process.

The proposed mathematical model described in section 3 is validated with experimental results and is used for the rest of the study.

4.4 Results

The fluids considered in this analysis is shown in Table 4.2. The fluids are selected according to working temperature of the proposed system which is between 554 K and 664 K. As mentioned before, the solid filler used in this study is quartzite having density of 2500 kg/m^3 and specific heat of 830 J/kg-K.

Table 4.2 : Properties of heat transfer fluids considered in this study (Bonas et al., 2016).

Heat Transfer Fluid	Density (kg/m^3)	Specific Heat (J/kg-K)	Volumetric Heat Capacity (MJ/m^3-K)	Thermal Conductivity (W/m-K)	Working Temperature (^oC)
Pressurized Air (20 bar, 600 K)	11.6	1056	0.01	0.046	<1000
Supercritical CO_2 (80 bar, 600 K)	72	1140	0.08	0.04	<850
Sodium (liquid)	820	1290	1.06	60	285-873
Lead-Bismuth Eutectic	9500	120	1.14	15	285-1650
Synthetic Oils	850	2200	1.87	1	<400
Solar Salt	1790	1500	2.69	0.5	290-590
HITEC Salt	1870	1561	2.92	0.2	<538

In energy storage problems, the most important parameter for fluid is multiplication of its density and specific heat ρ x C_p which is called volumetric heat capacity (VHC). It defines how much energy can be carried with fluid from solar field to storage tank as well as percentage of energy stored in fluid and solid at every stage of the charge and/or discharge cycle. For the same operating conditions i.e. type and amount of solid filler, porosity, and temperature, each fluid results in different initial stored energy in the tank. Although it is not the commercial practice to use different fluids at the same thermal conditions due to the fact that each fluid has an operating temperature which provides the maximum efficiency to system, same thermal conditions and same velocity at inlet and outlet of the tank are assumed in this study to compare the effect of other parameters.

For the same charge temperature of 664 K, initial energy stored in the system before discharge cycle for each fluid is given in Figure 4.5. The trends in Figure 4.5 can be explained by using VHC values of fluids given in Table 4.2. For the same porosity value, it is clear that as VHC value of the fluid increases total energy stored in the system increases because of the high energy storage capacity fluid brings more energy

with it from the heat exchanger. The tank that is filled with HTEC Salt has the higher initial energy stored with VHC value of 2.9 whereas pressurized air has the lowest initial energy stored with VHC value of 0.01.

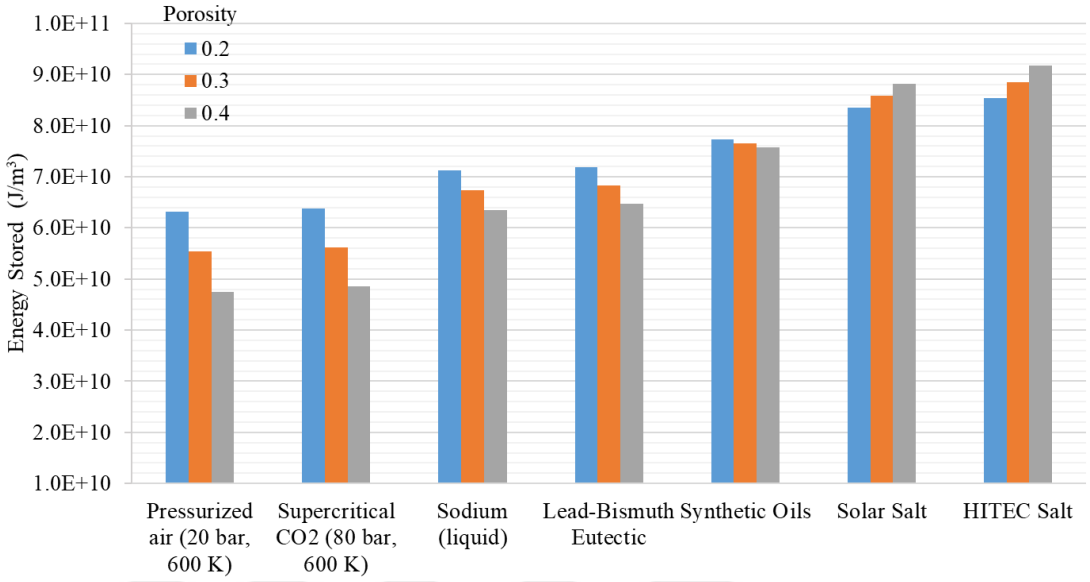

Figure 4.5 : Total energy stored in the tank before discharge.

Another result from Figure 4.5 is that as porosity increases total energy stored in the tank decreases except for cases when Solar Salt and HITEC Salt used as fluid. The reason of this trend is due to the fact that increase in porosity results in more fluid in the tank therefore reduces the total energy stored in the tank for systems where solid VHC value is higher than fluid VHC value. On the other hand, if solid filler material has VHC value less than the fluid then the amount of energy stored in the tank increases with porosity. In this study, VHC value of quartzite is 2.08 MJ/m^3-K which is less than VHC values of Solar Salt and HITEC Salt. The percentage of total initial energy stored in solid is given in Figure 4.6. It is clear from the figure that for the same porosity value, when the fluid VHC value decreases more energy is stored in the solid filler material. This is the desired operation since solid filler material is considered as the main storage component of the system.

Another fact shown in Figure 4.6 is that when porosity increases, energy stored in solid decreases due to the fact that amount of fluid in the tank increases with high value of porosity. This decrease is more significant when solid and fluid materials have comparable VHC values.

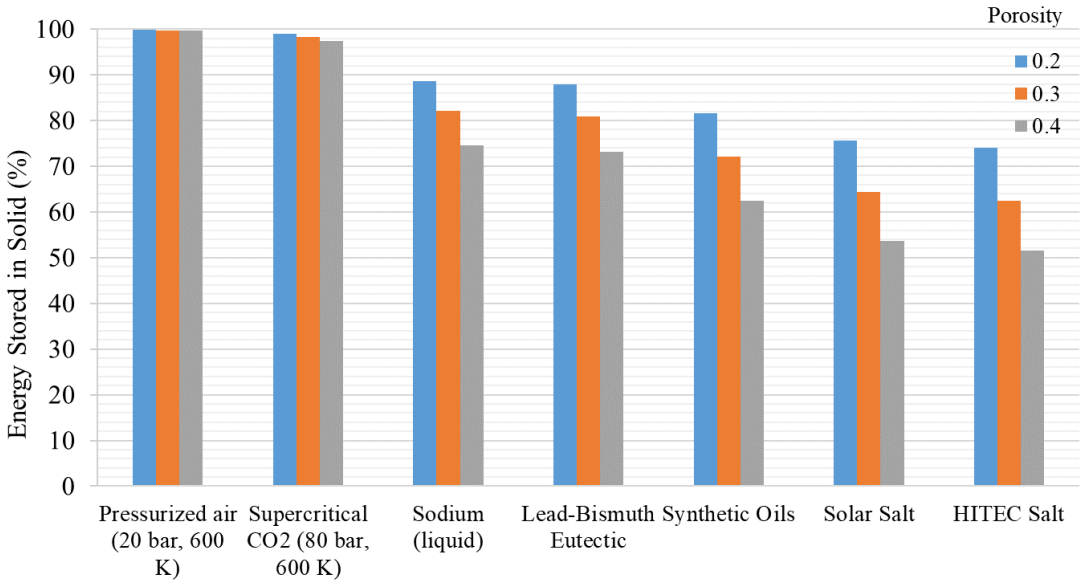

Figure 4.6 : Fraction of energy stored in solid filler before discharge.

4.4.1 Sensitivity study on porosity and sphericity

For each fluid in Table 4.2, the effect of different porosity and sphericity values on the discharge process was investigated with sensitivity analysis. The energy remained in the tank after 3 hours of discharge for all fluids are given in Figure 4.7 to Figure 4.13.

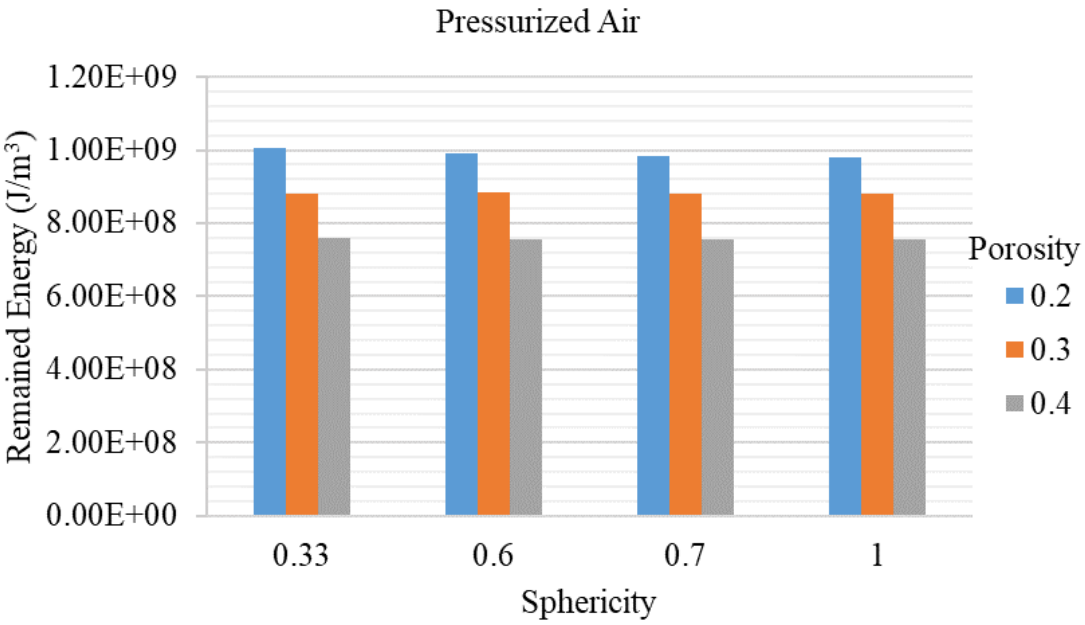

Figure 4.7 : The energy remained in tank after 3 h of discharge for Pressurized Air.

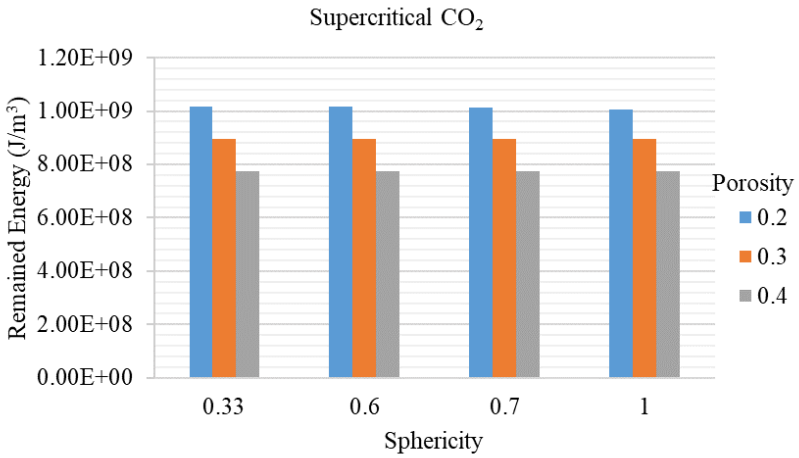

Figure 4.8 : The energy remained in tank after 3 h of discharge for Supercritical CO_2.

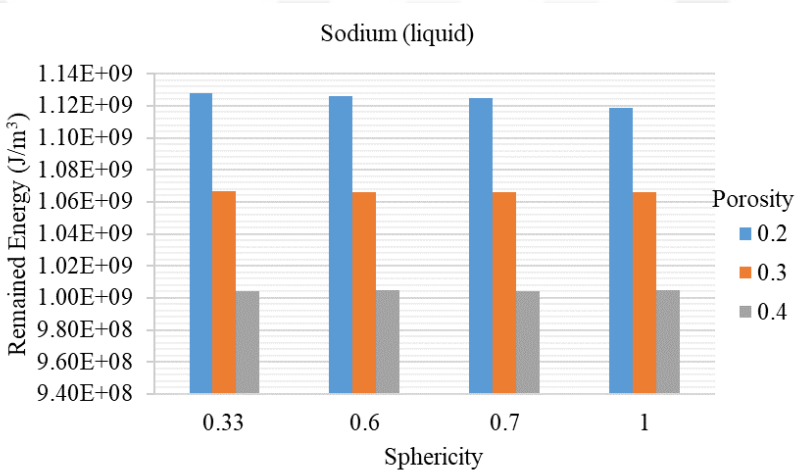

Figure 4.9 : The energy remained in tank after 3 h of discharge for Sodium (liquid).

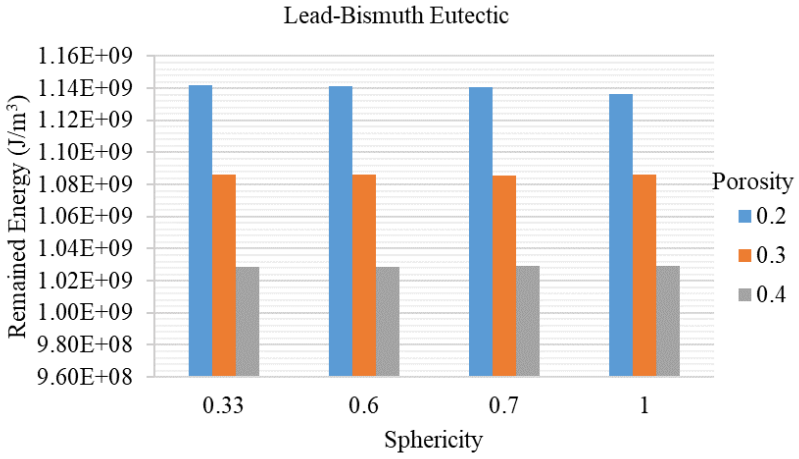

Figure 4.10 : The energy remained in tank after 3 h of discharge for Lead-Bismuth Eutectic.

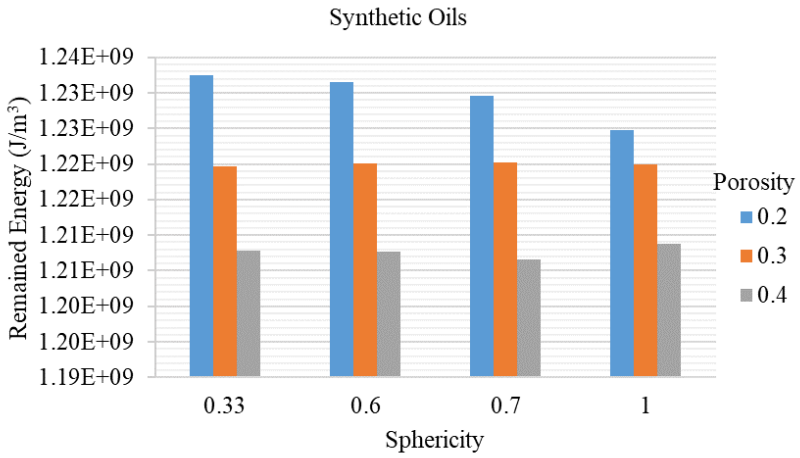

Figure 4.11 : The energy remained in tank after 3 h of discharge for Synthetic Oils.

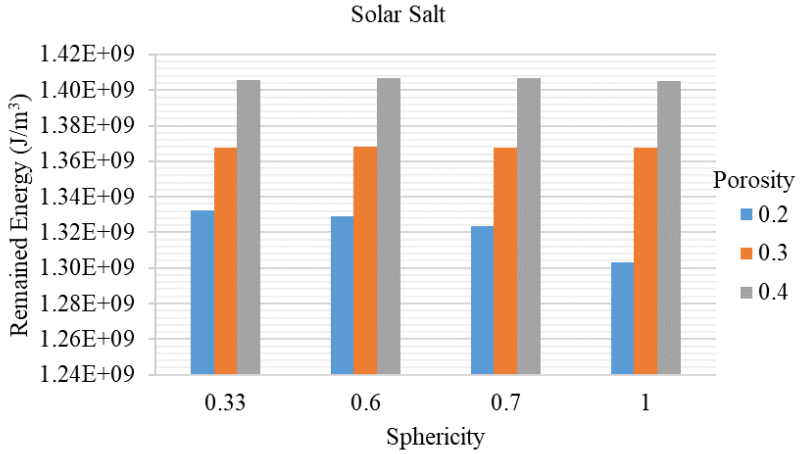

Figure 4.12 : The energy remained in tank after 3 h of discharge for Solar Salt.

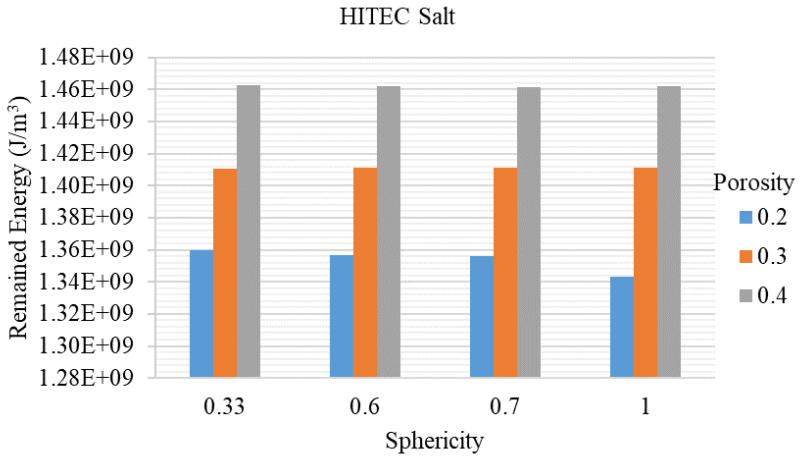

Figure 4.13 : The energy remained in tank after 3 h of discharge for HTEC Salt.

It is clear from above figures that as fluid VHC increases, the energy remained in the tank increases. This increase is more pronounced for fluids having VHC values greater

than the solid filler material. The trend does not change with different porosity or sphericity values. On the other hand, increase in porosity decreases the amount of energy remained in the tank for all cases except for the cases where Solar Salt and HTEC Salt used as working fluid. It should be noted that when solid has VHC value higher than the fluid, it acts as the main storage component of the system. During the discharge cycle, solid filler transfers the energy to cold fluid efficiently and energy remained in the tank decreases. On the other hand, when fluid acts as main storage component of the system which is when fluid has higher value of VHC than solid filler material, cold fluid does not receive enough energy from solid. The effect of sphericity on the discharge process can only be seen when the porosity value is 0.2. For this case, increase in sphericity results in decrease in energy remained in the tank. The power generated during 3 hours of discharge cycle is given in Table 4.3. The values in Table 4.3 are calculated by taking the difference between initial energy of the tank and energy remained in the tank. The maximum power generated for all fluids is when sphericity is equal to 1 and porosity is equal to 0.2. Porosity has negative effect on total power generated from the tank on the contrary sphericity seems to have positive effect.

Table 4.3 : Power of the tank after 3 hours of discharge (MW).

Working Fluid	Porosity	Sphericity			
		0.33	0.6	0.7	1.0
Pressurized Air (20 bar, 600 K)	0.2	0.501	0.574	0.612	0.636
	0.3	0.443	0.434	0.439	0.445
	0.4	0.370	0.374	0.375	0.376
Supercritical CO_2 (80 bar, 600 K)	0.2	0.499	0.506	0.513	0.554
	0.3	0.443	0.444	0.443	0.443
	0.4	0.379	0.381	0.385	0.379
Sodium (liquid)	0.2	0.592	0.601	0.608	0.639
	0.3	0.561	0.562	0.562	0.563
	0.4	0.533	0.531	0.532	0.531
Lead-Bismuth Eutectic	0.2	0.574	0.642	0.578	0.664
	0.3	0.545	0.635	0.547	0.634
	0.4	0.521	0.636	0.517	0.637
Synthetic Oils	0.2	0.609	0.613	0.624	0.649
	0.3	0.604	0.602	0.602	0.603
	0.4	0.596	0.596	0.602	0.591
Solar Salt	0.2	0.653	0.669	0.696	0.803
	0.3	0.679	0.676	0.678	0.678
	0.4	0.691	0.687	0.686	0.694
HITEC Salt	0.2	0.671	0.687	0.691	0.756
	0.3	0.698	0.695	0.694	0.696
	0.4	0.720	0.724	0.725	0.724

In order to compare the distribution of total energy remained in the tank between fluid and solid, 3 fluids having minimum, intermediate and maximum VHC values in Table 4.2 were selected. Percent energy stored in solid for Pressurized Air which has the lowest VHC value, Sodium (liquid), and Solar Salt which has the highest VHC value are shown in Figure 4.14 to Figure 4.16.

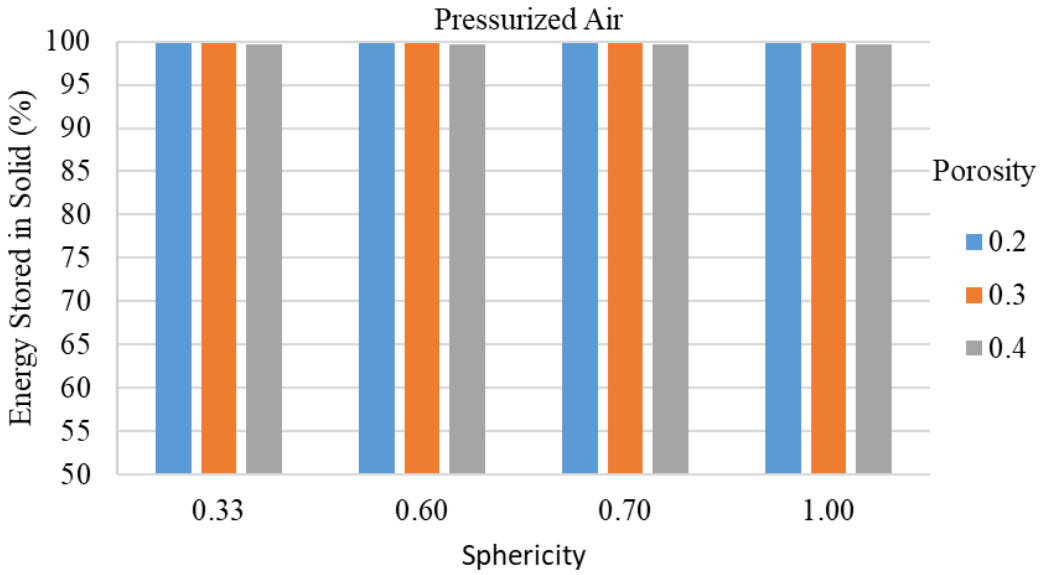

Figure 4.14 : Fraction of energy stored in solid filler after 3 hours of discharge for Pressurized Air.

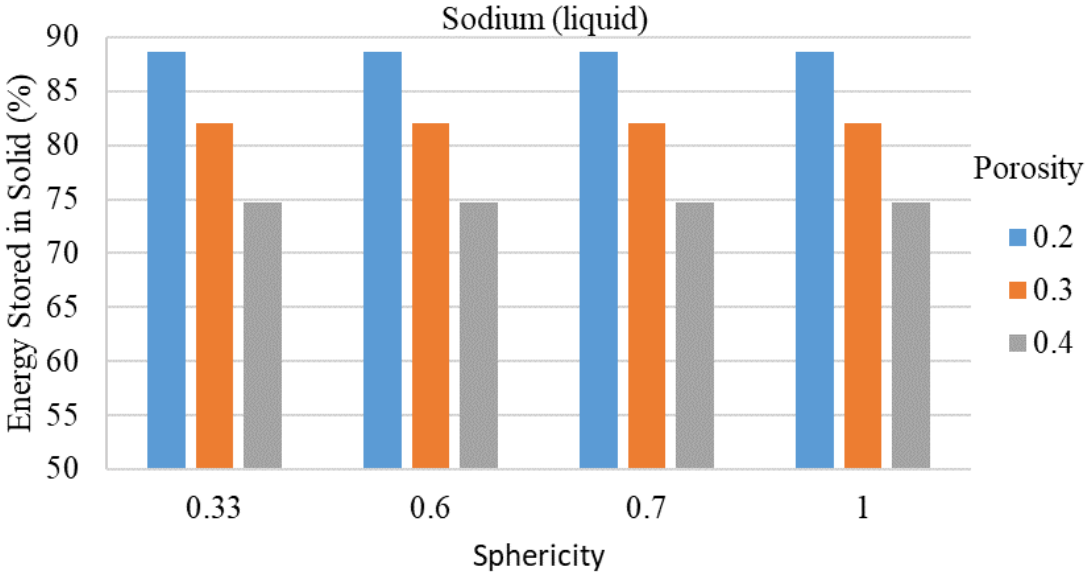

Figure 4.15 : Fraction of energy stored in solid filler after 3 hours of discharge for Sodium (liquid).

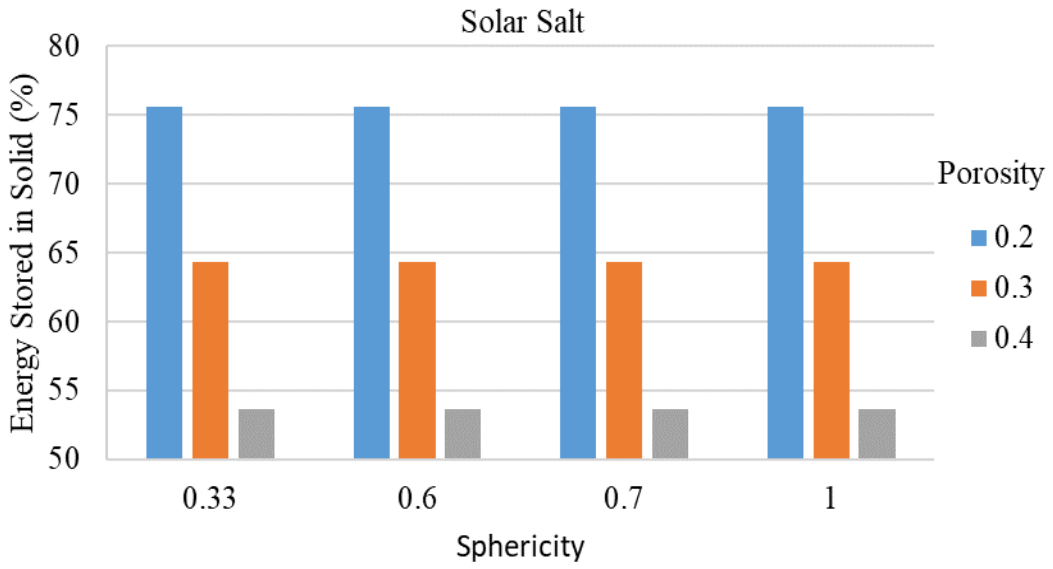

Figure 4.16 : Fraction of energy stored in solid filler after 3 hours of discharge for Solar Salt.

It is clear from above figures that solid filler material in the tank where Pressurized Air used as fluid still contains the majority of the total energy remained in the tank. As at the beginning of discharge, increase in porosity decreases percent energy stored in solid filler material and sphericity does not have significant effect.

4.4.2 Streamlines, temperature and velocity profiles

Velocity and temperature profiles and streamlines at various porosity and sphericity values for selected fluids from Table 4.2 according to their VHC values are discussed in this section. All the figures are given in Appendix A. As described above, fluids with low (Pressurized Air), medium (Sodium (liquid)), and high (Solar Salt) VHC values are used for the analysis.

At discharge, streamlines preferred to be either uniform or close to uniform to prevent mixing of hot and cold fluids. Because, when clod and hot fluid is mixed, power of the tank decreases. Rather than giving information about the power of the tank at certain time at discharge, streamline, velocity and temperature analysis provides good opportunity to understand behavior of the tank with time.

It is seen from the figures in Appendix A that streamlines are much more uniform for all liquids when porosity is equal to 0.2 and sphericity is equal to 1. This indicates less mixing in the tank and temperature profiles support this outcome. The discharge process can clearly be seen from temperature profiles that cold fluid moved from the

bottom of the tank towards to top and there is a clear distinction between the cold and hot fluids. The difference between the maximum and minimum temperature in the tank is highest at this case again showing less mixing in the tank. The velocity profile is similar to streamlines.

4.4.3 Time dependent behavior of tank during discharge

The discharge process duration at simulations increased to 6 hours to understand the time behavior of the stored energy in the storage tank for parameters under investigation. Three different fluids Pressurized Air, Sodium (liquid) and Solar Salt were selected again according to their VHC values.

The variation of stored energy in the tank with time is shown in Figure 4.17 to Figure 4.20 for all fluids. The results are presented with same sphericity per graph first to estimate the effect of porosity. The increase in porosity results in a decrease in stored energy for all sphericity cases.

The slope of the lines in Figure 4.17 to Figure 4.20 depends on time and indicates the discharge power of the tank. The slopes decrease as discharge process advances in time therefore outlet velocity must be increased to keep the discharge power constant.

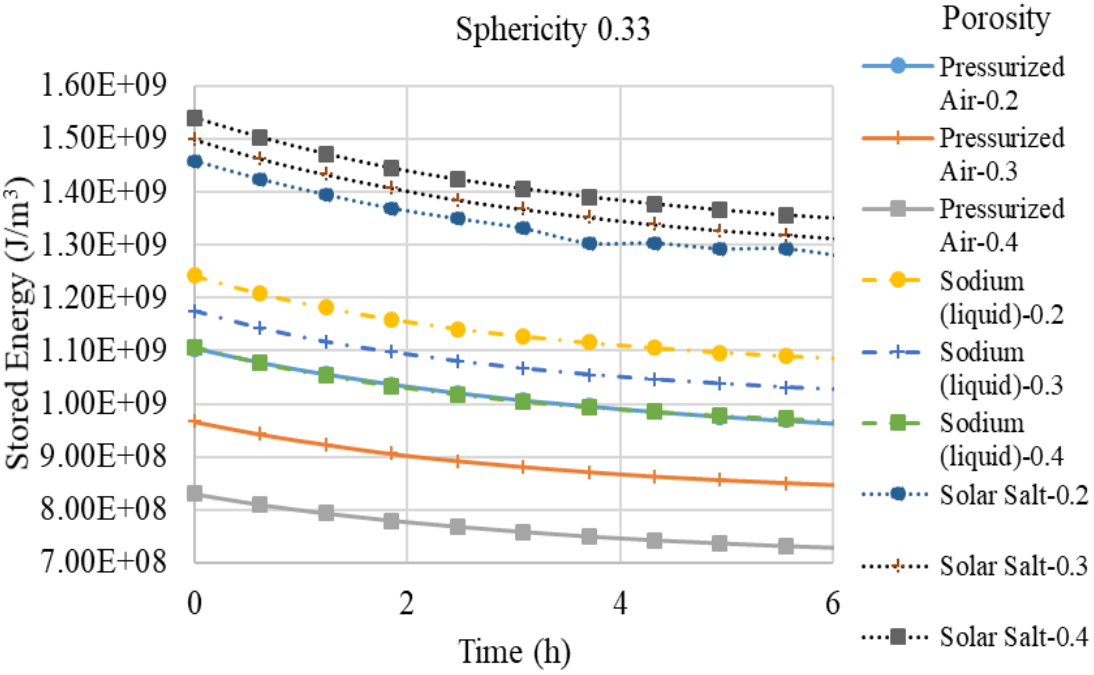

Figure 4.17 : Variation of stored energy in the tank with time during discharge for sphericity 0.33.

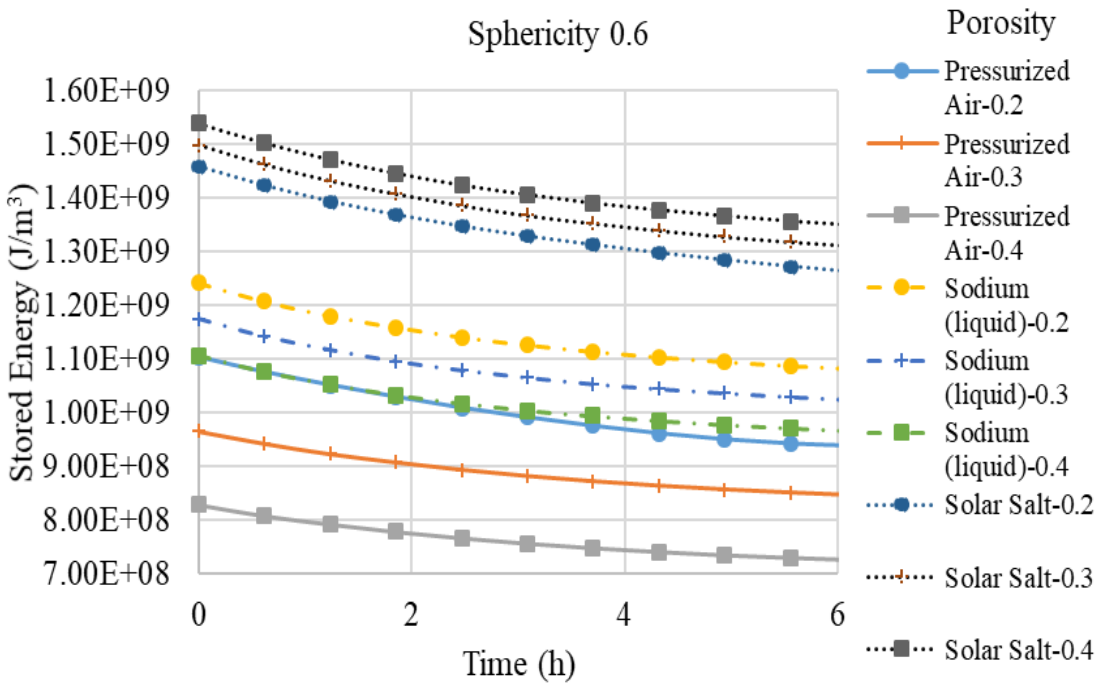

Figure 4.18 : Variation of stored energy in the tank with time during discharge for sphericity 0.6.

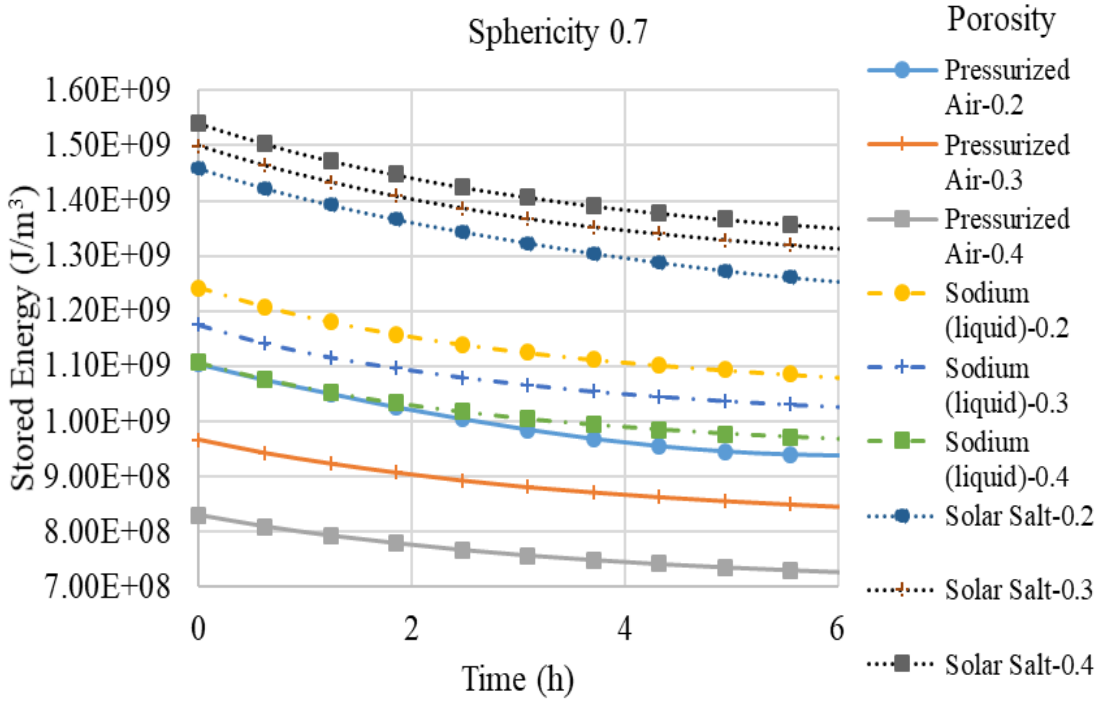

Figure 4.19 : Variation of stored energy in the tank with time during discharge for sphericity 0.7.

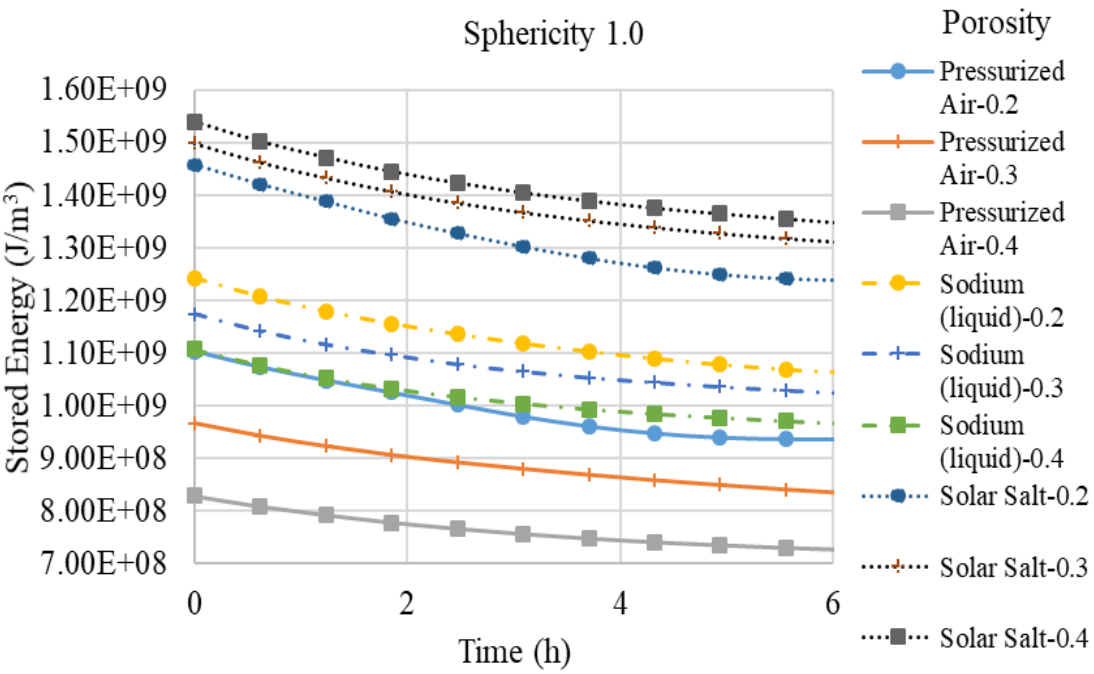

Figure 4.20 : Variation of stored energy in the tank with time during discharge for sphericity 1.0.

The same results were rearranged to see the effect of sphericity on the final stored energy. As mentioned before the effect is significant only when the porosity is 0.2 therefore only the results of this case is presented. The stored energy decreases with high value of sphericity according to Figure 4.21, Figure 4.22, and Figure 4.23.

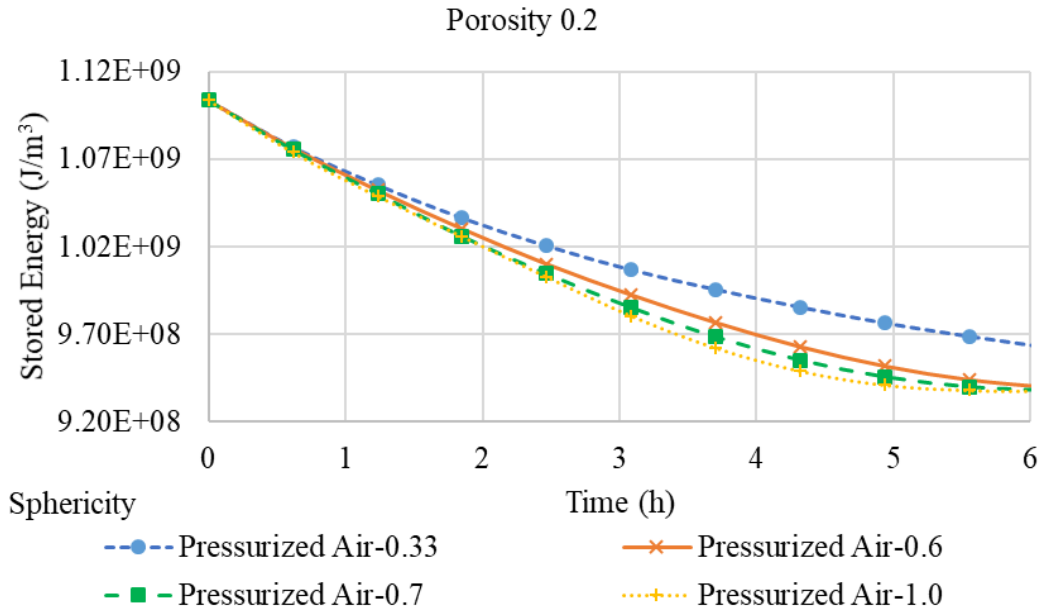

Figure 4.21 : Variation of stored energy in the tank with time during discharge for Pressurized Air for porosity 0.2.

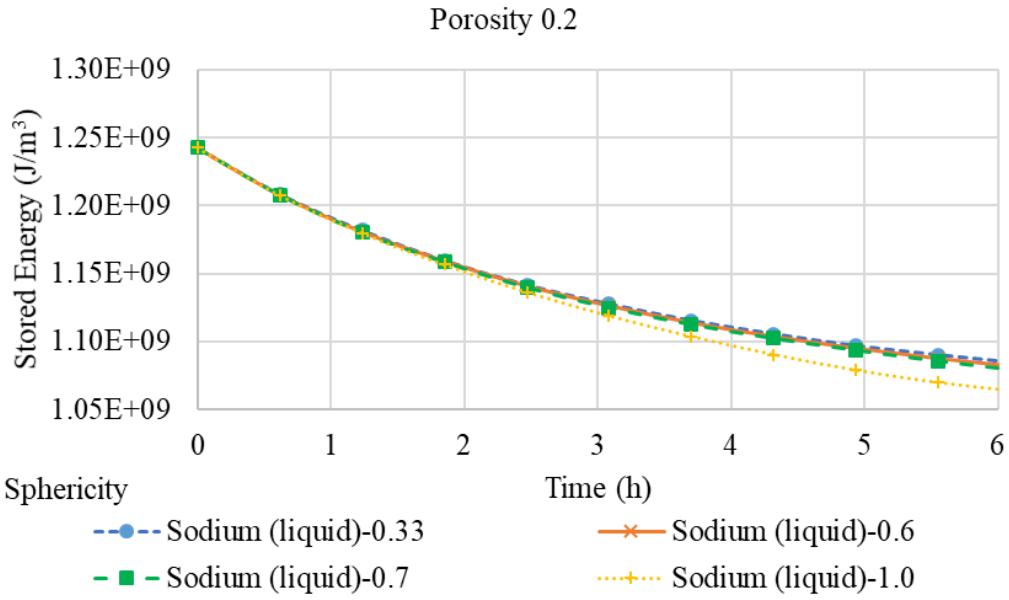

Figure 4.22 : Variation of stored energy in the tank with time during discharge for Sodium (liquid) for porosity 0.2.

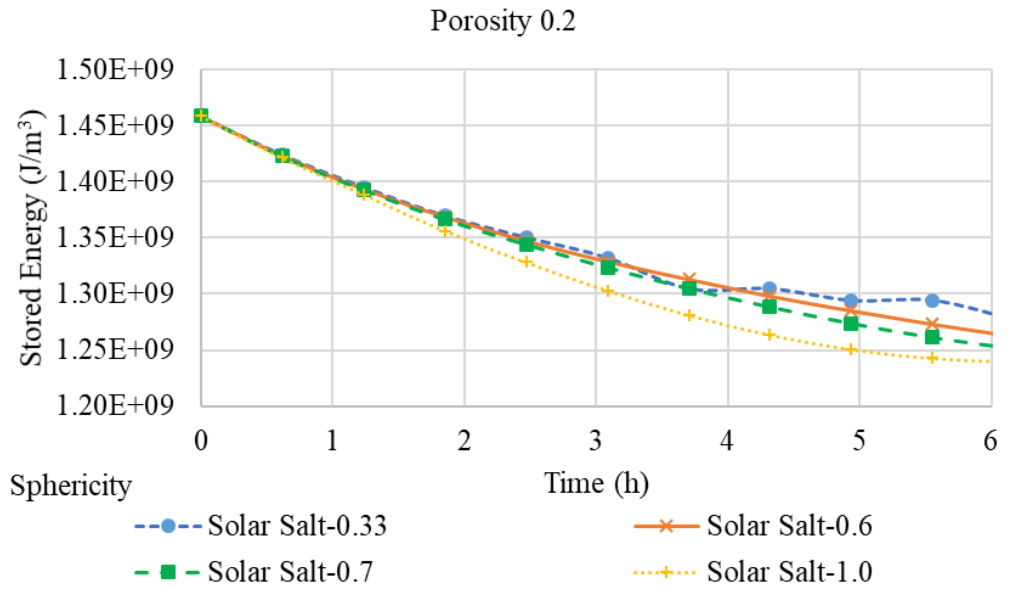

Figure 4.23: Variation of stored energy in the tank with time during discharge for Solar Salt for porosity 0.2.

Time dependent behaviour of Pressurized Air and Solar Salt are also discussed in detail at this section since they have the lowest and highest volumetric heat capacity value. Temperature profiles and streamlines of both fluids at every 30 minutes of the simulations are given in Appendix B. In order to see the effect of minimum and maximum values of porosity and sphericity, porosity values of 0.2 and 0.4 and sphericity values of 0.33 and 1 were taken into consideration. According to the figures in Appendix B, increasing sphericity value prevents non-uniformity therefore results

in good discharge performance. On the other hand, increasing porosity causes mixing of hot and cold fluid no matter what the value of the sphericity is. This means energy loss at the tank. At figures which present axial distribution of temperature at tank midline, an unusual treatment of lines is obvious, thermocline range is increased and at some cases thermocline cannot be determined. That situation means less efficiency of tank and correspond the combination of porosity and sphericity discussed above.

5. CONCLUSIONS AND RECOMMENDATIONS

In this work, the aim was to investigate the effect of various parameters on single-tank thermocline energy storage system discharge performance to provide insight to selection process of operation parameters and materials for the system. The simulations were performed with computational fluid dynamics to fully integrate the mathematical models into calculations without any simplification. Seven different working fluids, three different porosity values, and finally four different sphericity values were considered for parametric study. Energy stored, velocity and temperature profiles, and streamlines in the tank after 3 hours of discharge process were presented. In addition, 6 hours of discharge was simulated to understand the timeline of the discharge process.

The simulation results indicate that the most important parameter for the storage system is how close volumetric heat capacity (VHC) value of the working fluid is close to value for solid filler material. This parameter changes the behavior of the tank completely. For example, if the fluid VHC value is higher than the solid filler material, increase in porosity increases the amount of remaining energy in the tank. Conversely, for other fluids which have VHC value lower than solid filler material, increase in porosity reduces the amount of remaining energy in the tank.

The effect of sphericity on the tank performance is not significant for high values of porosity. For the smallest value considered in this study, increase in sphericity resulted in decrease in amount of remaining energy in the tank. On the other hand, temperature profiles and streamlines of the 6 hours of discharge showed that for low values of porosity, higher sphericity value prevents mixing of hot and cold fluid and results in better discharge performance.

The fluid with the highest VHC value has the greatest discharge power among all fluids. The discharge speed increase with increasing sphericity and decreasing porosity due to the fact that since permeability, which defines resistance of solid against fluid flow, depends on porosity, sphericity, and solid particles diameter (treated constant in this study) reduction in permeability results in increase in resistance.

The investigation of streamlines showed that eddies and vortexes get larger and they divide the tank into two or more regions. These regions are not connected to each other as convection type therefore heat transfer between them happens just as conduction type. As a result, heat transfer and discharge ratio get smaller.

REFERENCES

Bejan A. 1982, Second-law analysis in heat transfer and thermal design.

Brenna M, Foiadelli F, Roscia M, Zaninelli D, 2008, Evaluation of solar collector plant to contribute climate change mitigation, Proceedings of the IEEE international conference sustainable energy technology, ICSET.

Brosseau D, Hlava P, Kelly M. 2004. Testing Thermocline Filler Materials and Molten-salt Heat Transfer Fluids for Thermal Energy Storage Systems Used in Parabolic Trough Solar Power Plants. Sandia National Laboratories, Albuquerque NM, Technical Report, 3207.

Bonanos A.M, Votyakov E.V, 2016. Sensitivity analysis for thermocline thermal storage tank design, International Journal of Heat and Mass Transfer, **37**, 939-954.

Bayon R, Rojas E. 2013, Simulation of thermocline storage for solar thermal power plants: from dimensionless results to prototypes and real-size tanks, International Journal of Heat and Mass Transfer, **60**, 713-721.

Brown N, Lai F. 2011, Enhanced thermal stratification in a liquid storage tank with a porous manifold. Solar Energy, **85**, 1409-1417.

Chang Z, Li X, Xu C, Chang C, Wang Z. 2014, The design and numerical study of a 2 MWh molten salt thermocline tank. Proceedings of Solar PACES.

Forsberg C, Peterson P, Zhao H. 2007, High-temperature liquid-fluoride-salt closed-brayton-cycle solar power towers. Journal of Solar Energy Engineering, **129**,141-146.

Flueckiger S, Yang Z. 2013, Review of molten-salt thermocline tank modeling for solar thermal energy storage. Heat and Mass Transfer Engineering, **34**, 787-800.

Gil A, Medrano M, Martorell I, Lazaro A, Dolado P, Zalba B, Cabeza L. 2010. State of the art on high temperature thermal energy storage for power generation. Renewable and Sustainable Energy Reviews, **14**, 31-55.

Gupta PK, 1999, Renewable energy sources-a long way to go in India. Renewable Energy, **16**, 1216-1219.

Gharbia N, Derbalb H, Bouaichaouia S, Said N. 2011, A comparative study between parabolic trough collector and linear Fresnel reflector technologies. Energy Procedia, **6**, 565-572.

Haller M, Cruickshank C, Streicher W, Harrison S, Andersen E, Furbo S. 2009, Methods to determine stratification efficiency of thermal energy storage processes e review and theoretical comparison. Solar Energy, **83,** 1847-1860.

Li P., Lew J.V, Karaki W, Chan C, Stephens J, Wang Q. 2011 Generalized charts of energy storage effectiveness for thermocline heat storage tank design and calibration. Solar Energy, **85**, 2130-2143.

Kolb G, Ho C, Mancini T, Gary J. 2011. Power Tower Technology Roadmap and CostReduction Plan. Sandia National Laboratories, Albuquerque NM, Technical Report 2419.

Kuznetsov A. 1995, An analytical solution for heating a two-dimensional porous packed bed by a non-thermal equilibrium fluid flow. Applied Science Research, **55**, 83-93.

Kuravi S, Trahan J, Goswami D, Rahman M, Stefanakos E. 2013, Thermal energy storage technologies and systems for concentrating solar power plants. Progress in Energy and Combustion Science, **39**, 285-319.

Kaushika ND, Reddy KS, 2000, Performance of a low cost solar paraboloid dish steam generating system. Energy Conversation and Management, **41**, 713-726.

Khan J, Arsalan MH, 2016, Solar power technologies for sustainable electricity generation – a review, Renewable and Sustainable Energy Reviews, **55**, 414-425.

Khan J, Arsalan MH, 2016, Solar power technologies for sustainable electricity generation – a review, Renewable and Sustainable Energy Reviews, **55**, 414-425.

Mills D, 2004, Advances in solar thermal electricity technology. Solar Energy, **76**, 19-31.

Pacheco J, Showalter S, Kolb W. 2002, Development of a molten-salt thermocline thermal storage system for parabolic trough plants. Solar Energy, **124**, 153-159.

Pianosi F, Sarrazin F, Wagener T. 2015, A matlab toolbox for global sensitivity analysis. Environmental Model and Software, **70**, 80-85.

Siva Reddy V, Kaushik SC, Tyagi SK. 2012, Year round performance and economic evaluation of solar power plant for Indian tropical condition. Journal of Renewable and Sustainable Energy, **4**, 4-13.

Taghizadeh S, Asaditaheri A. 2018, Heat transfer and entropy generation of laminar mixed convection in an inclined lid driven enclosure with a circular porous cylinder. International Journal of Thermal Science, **134**, 242-257.

Votyakov E, Bonanos A. 2014, A perturbation model for stratified thermal energy storage tanks. International Journal of Heat and Mass Transfer, **75**, 218-223.

Votyakov E, Bonanos A. 2015, Algebraic model for thermocline thermal storage tank with filler material, Solar Energy, **122**, 1154-1157.

Xu C, Wang Z, He Y, Li X, Bai F. 2012, Sensitivity analysis of the numerical study on the thermal performance of a packed-bed molten salt thermocline thermal storage system, Applied Energy, **92**, 65-75.

Yang Z., Garimella S, 2010, Thermal analysis of solar thermal energy storage in a molten-salt thermocline, Solar Energy, **84**, 974-985.

Zurigat Y, Liche P, Ghajar A. 1991, Influence of inlet geometry on mixing in thermocline thermal energy storage. International Journal of Heat and Mass Transfer, **34**, 115-125.

APPENDICES

APPENDIX A: Streamlines, temperature and velocity profiles of Pressurized Air and Solar Salt after 3 hours of discharge.
APPENDIX B: Graphs of time dependent behaviour of Pressurized Air and Solar Salt.

APPENDIX A: Temperature profiles, stream-lines, and velocity profiles of Pressurized Air, Sodium (liquid) and Solar Salt after 3 hours of discharge

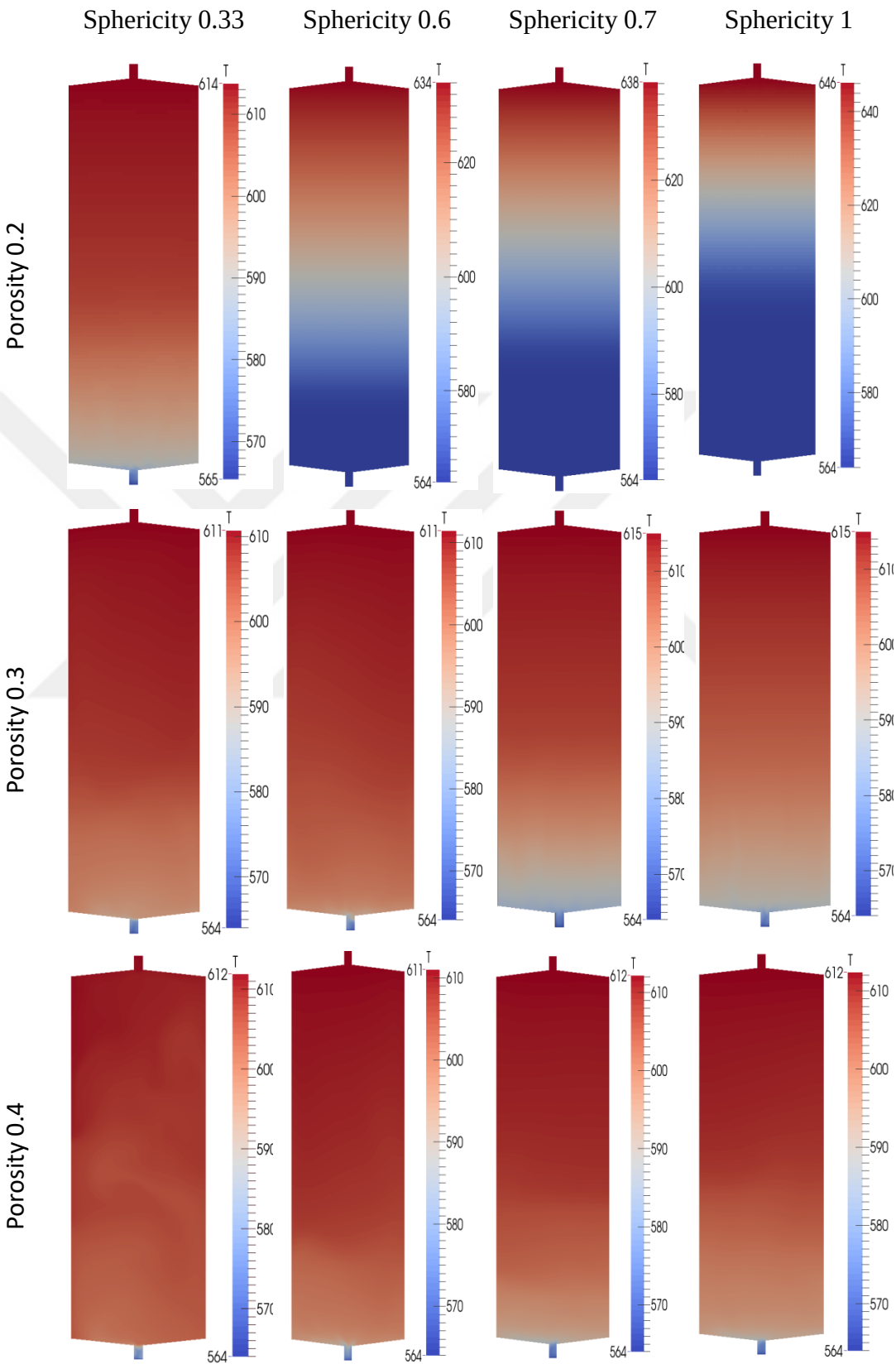

Figure A.1 : Temperature profile of Pressurized Air after 3 hours of discharge.

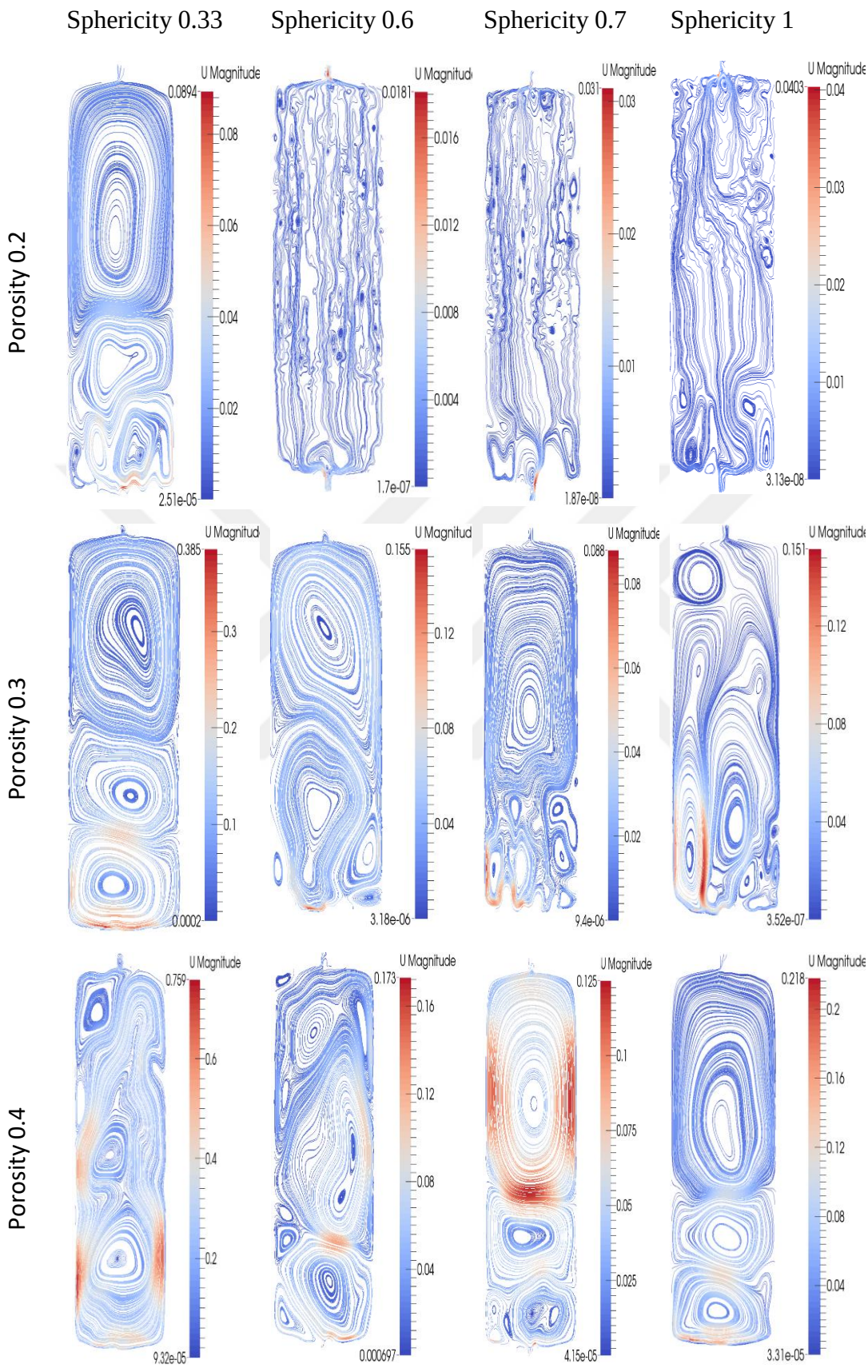

Figure A.2 : Streamlines of Pressurized Air after 3 hours of discharge.

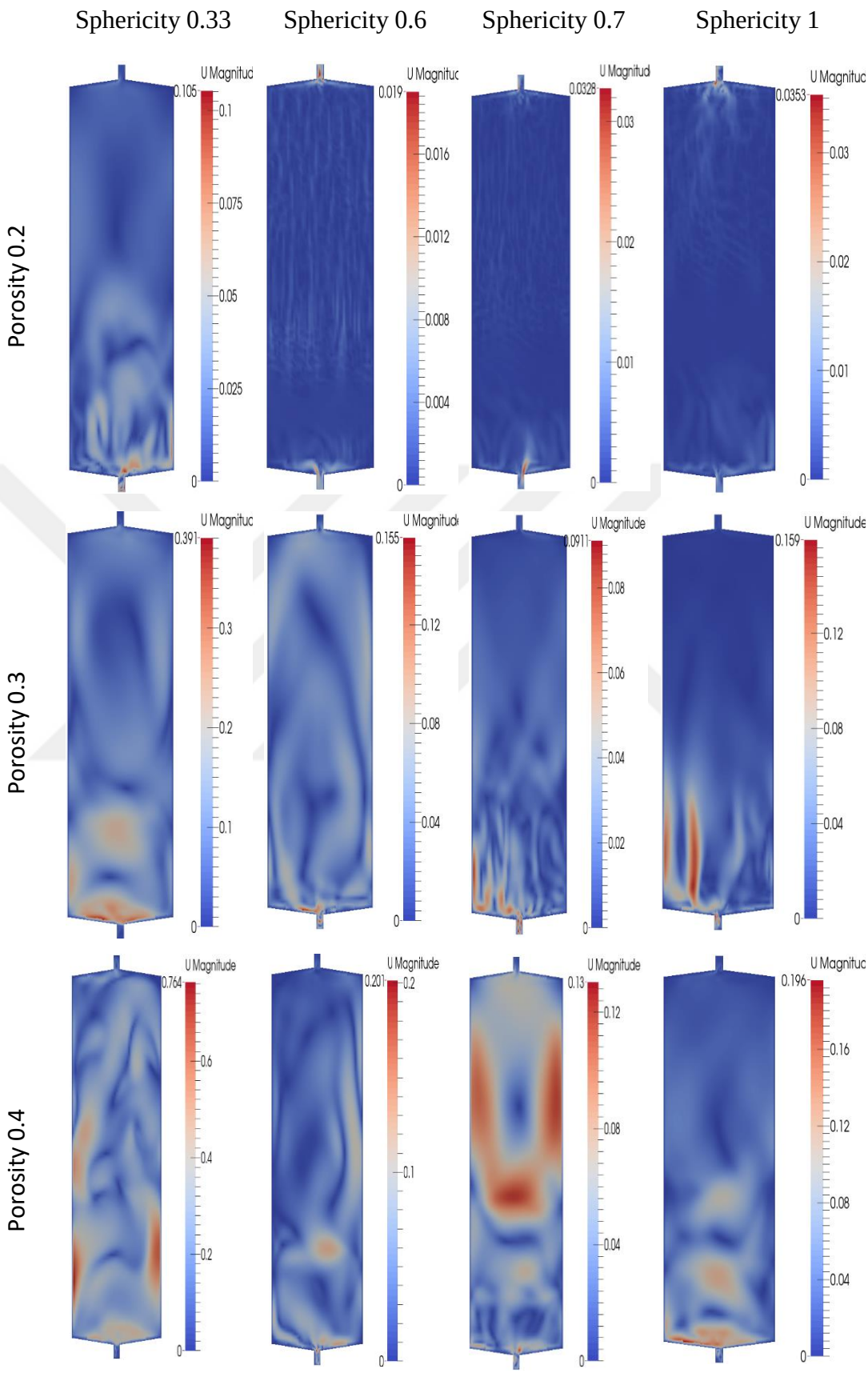

Figure A.3 : Velocity profile of Pressurized Air after 3 hours of discharge.

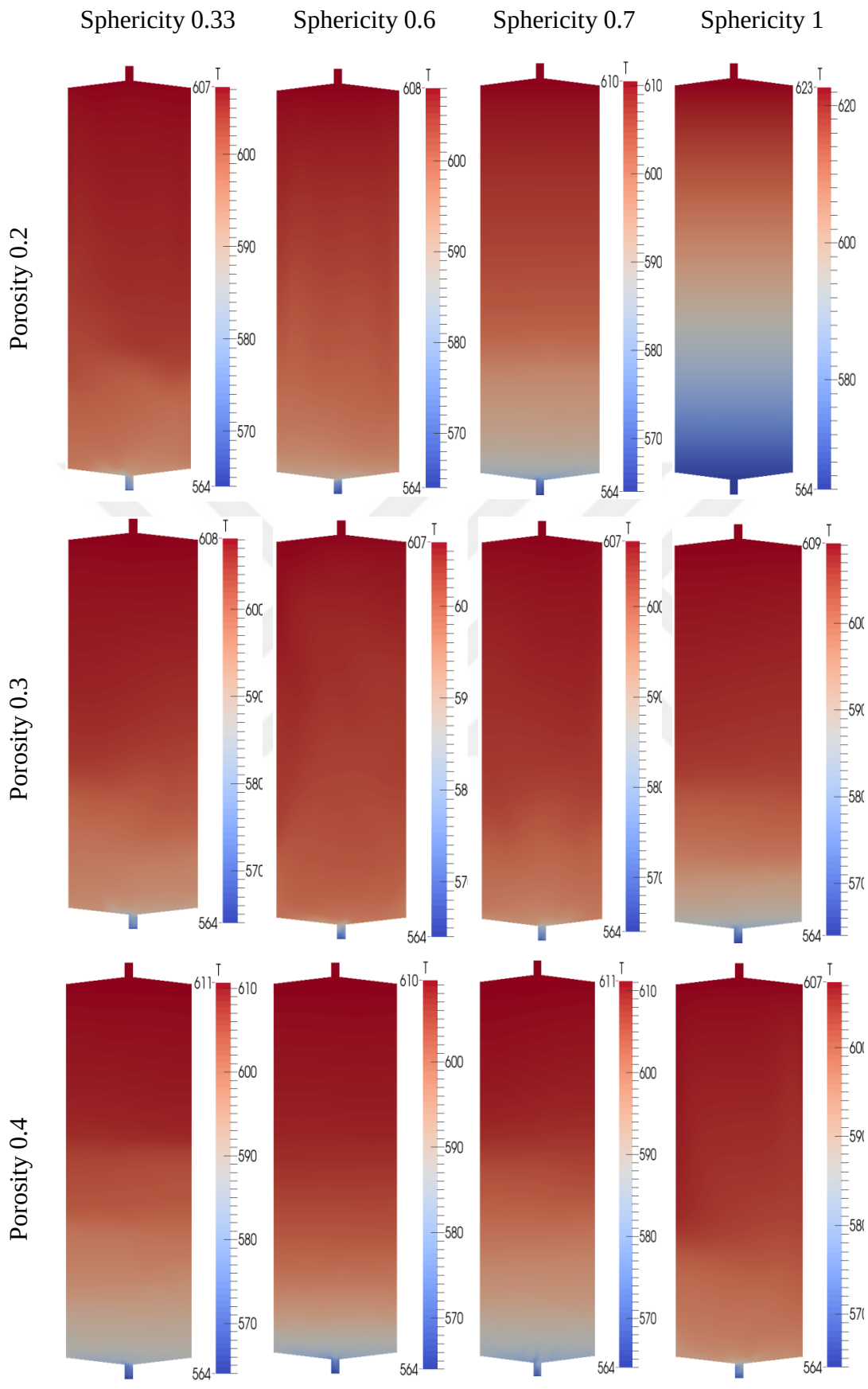

Figure A.4 : Temperature profile of Sodium (liquid) after 3 hours of discharge.

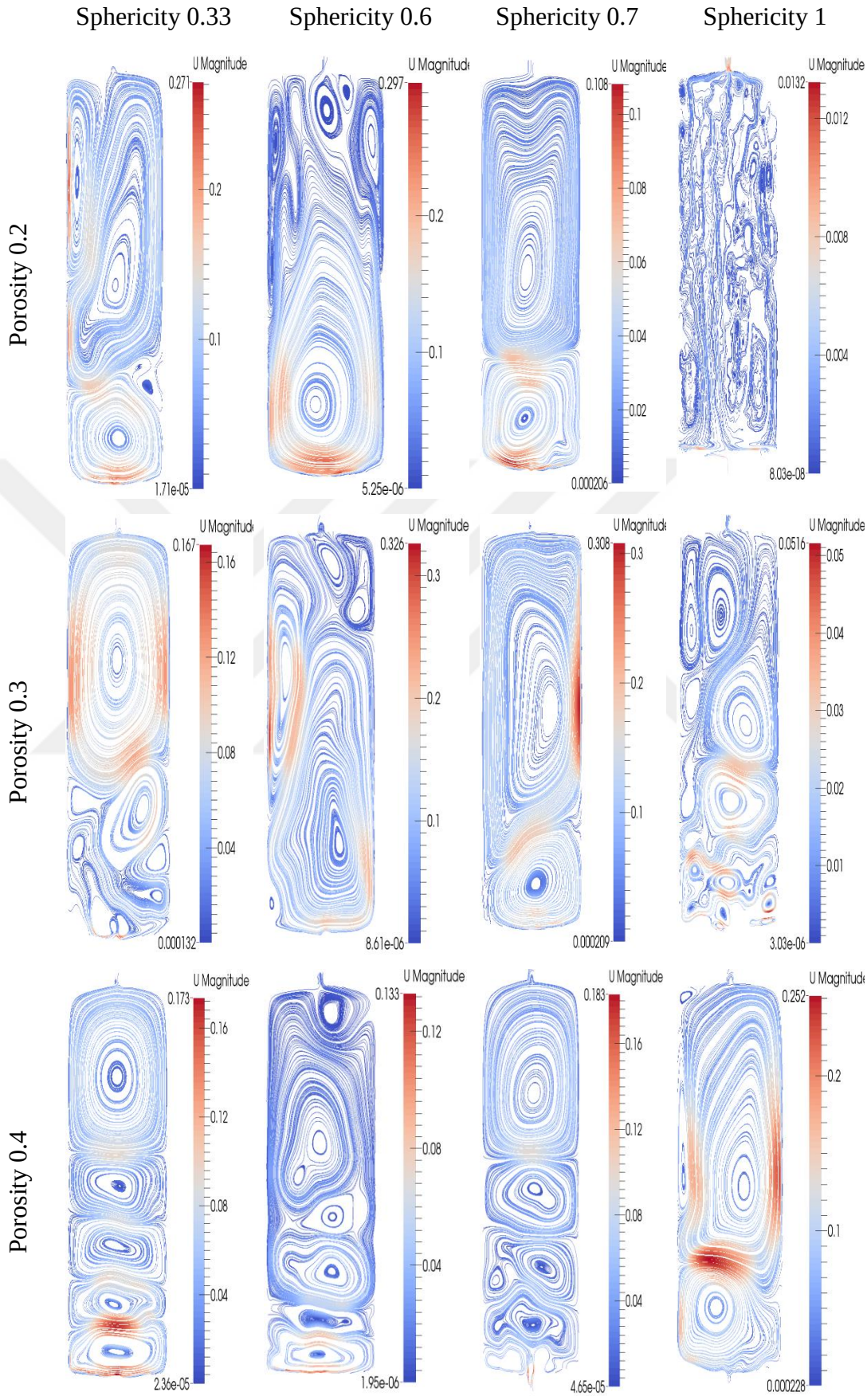

Figure A.5 : Streamlines of Sodium (liquid) after 3 hours of discharge.

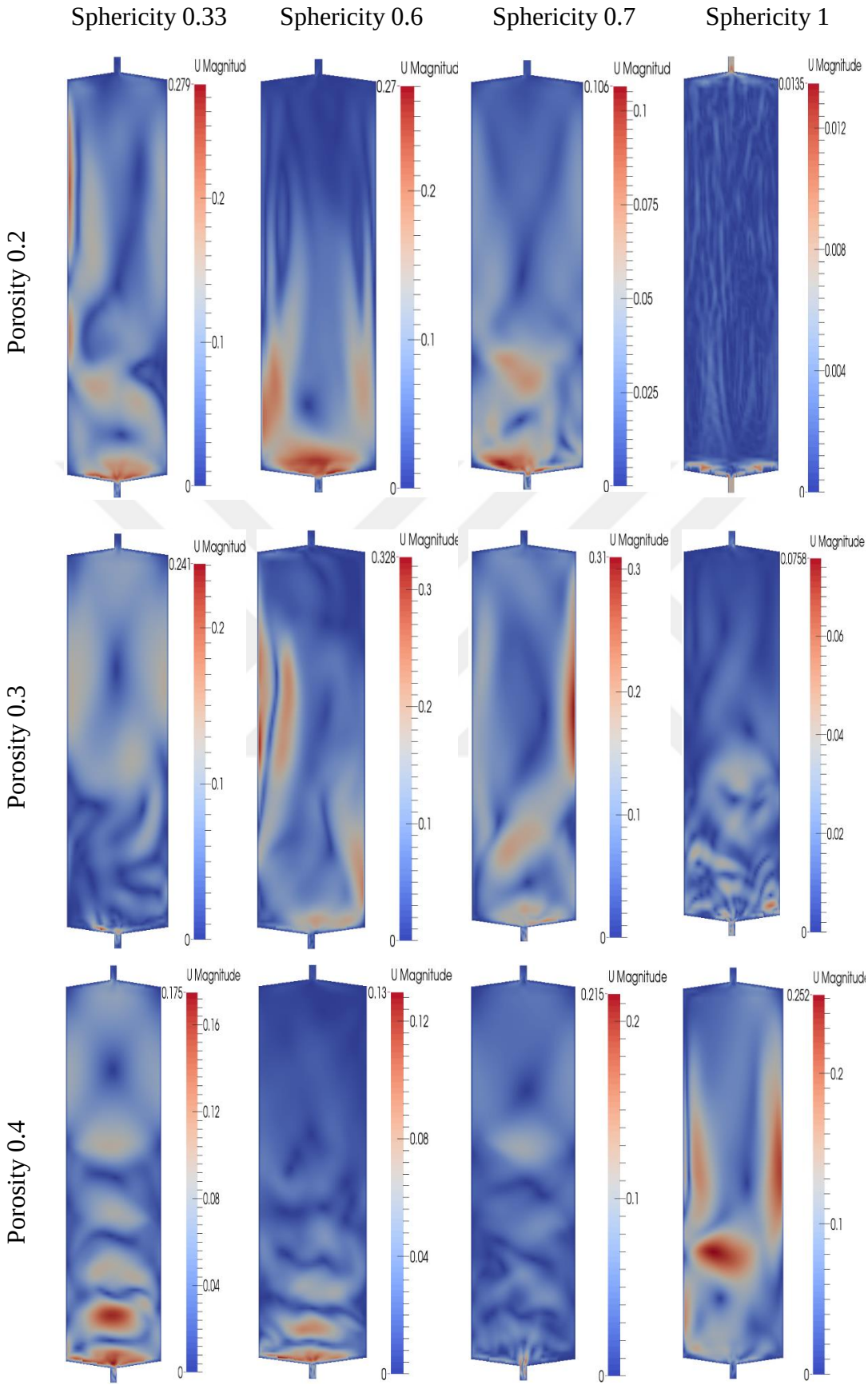

Figure A.6 : Velocity profile of Sodium (liquid) after 3 hours of discharge.

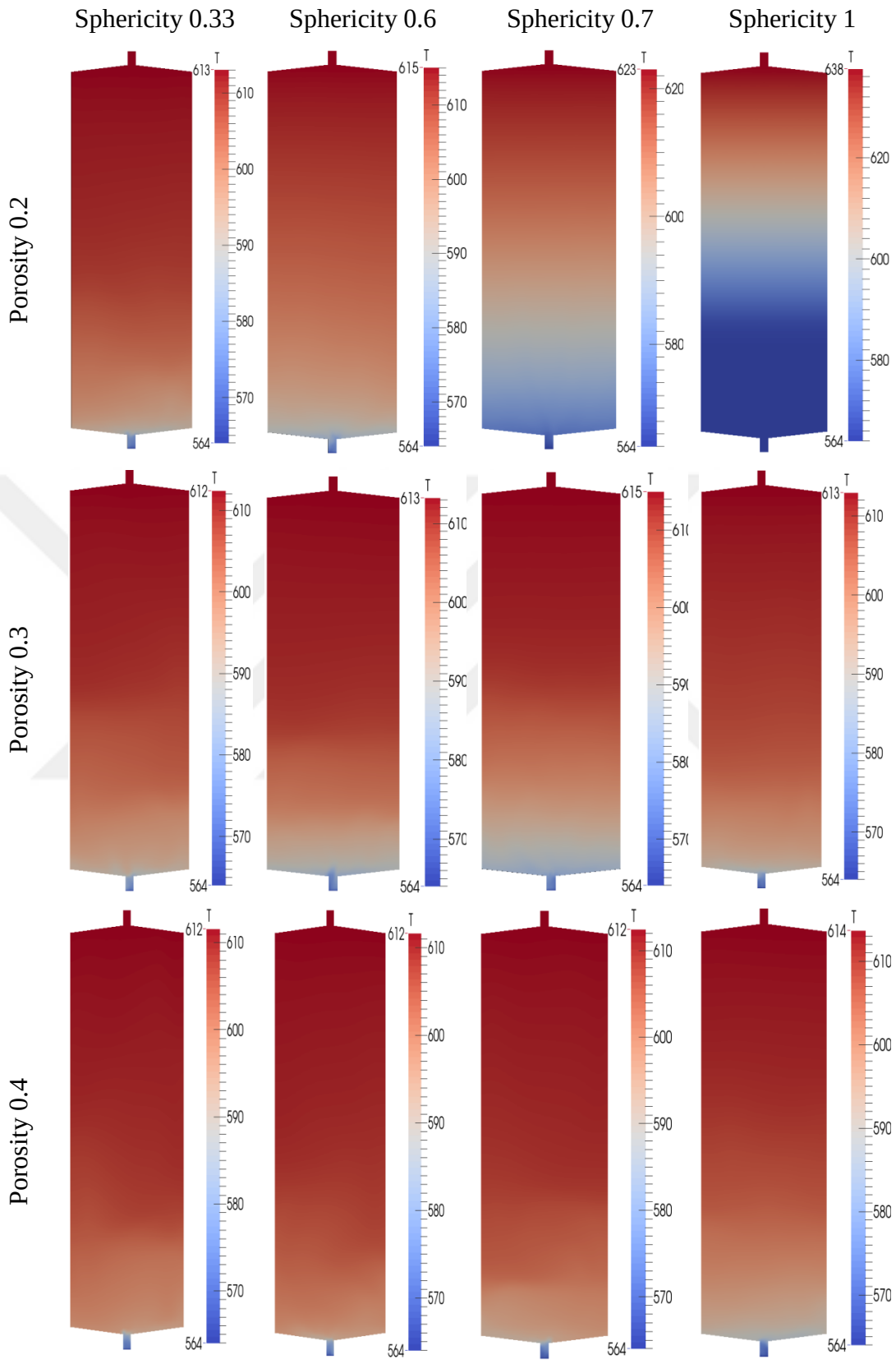

Figure A.7 : Temperature profile of Solar :Salt after 3 hours of discharge.

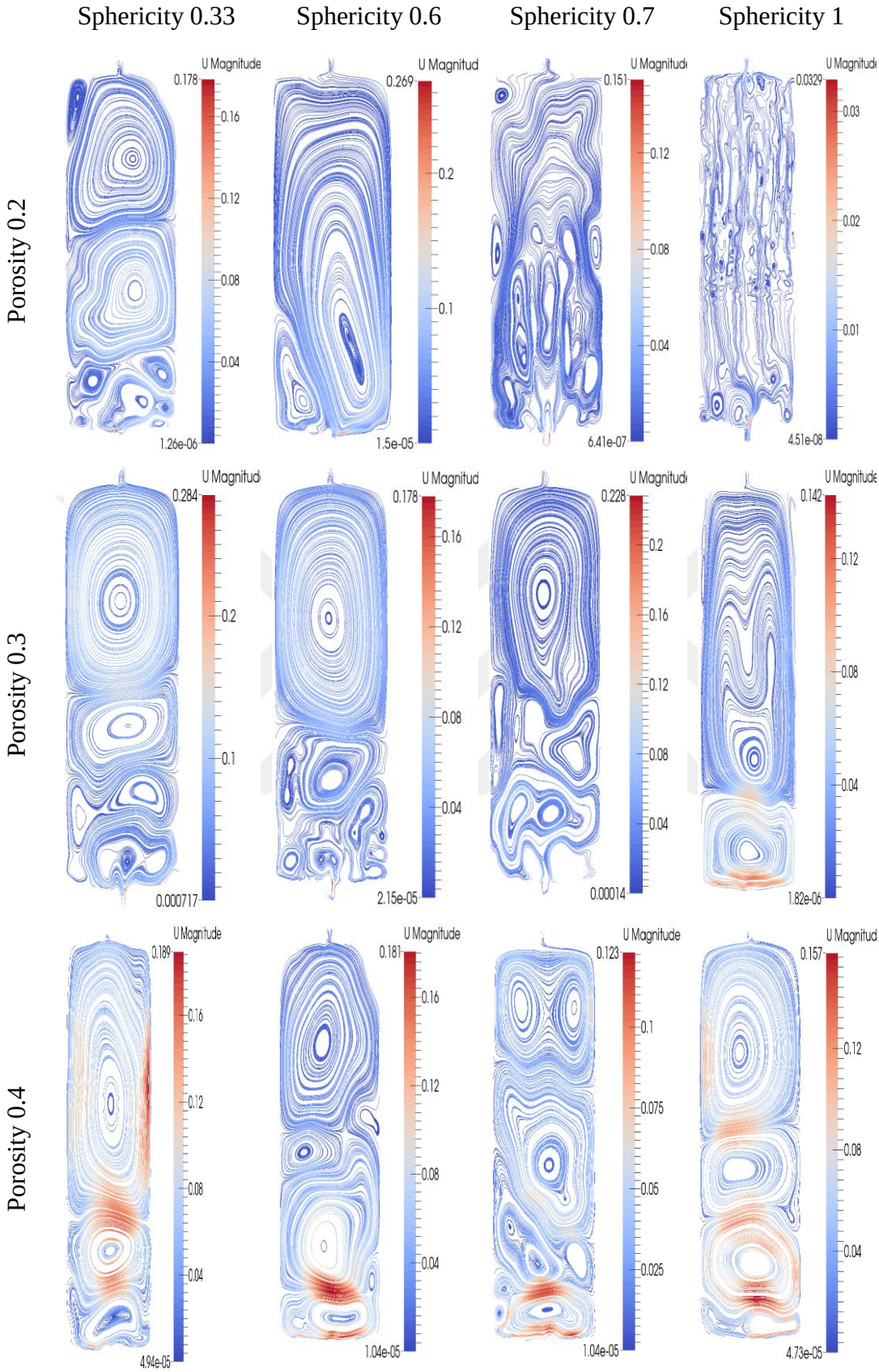

Figure A.8 : Streamlines of Solar :Salt after 3 hours of discharge.

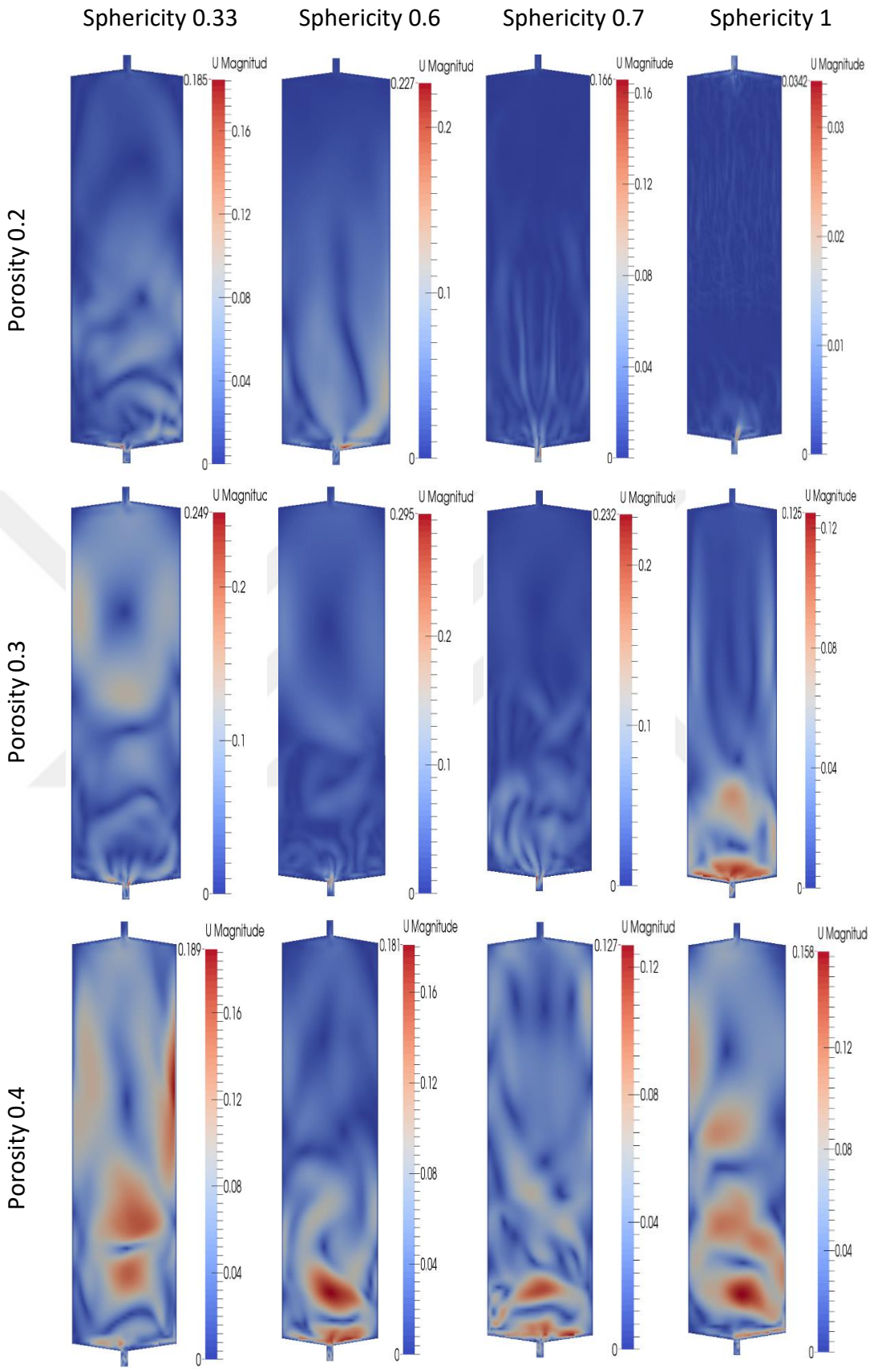

Figure A.9 : Velocity profile Solar :Salt after 3 hours of discharge.

APPENDIX B: Time dependent behaviour of Pressurized Air and Solar Salt.

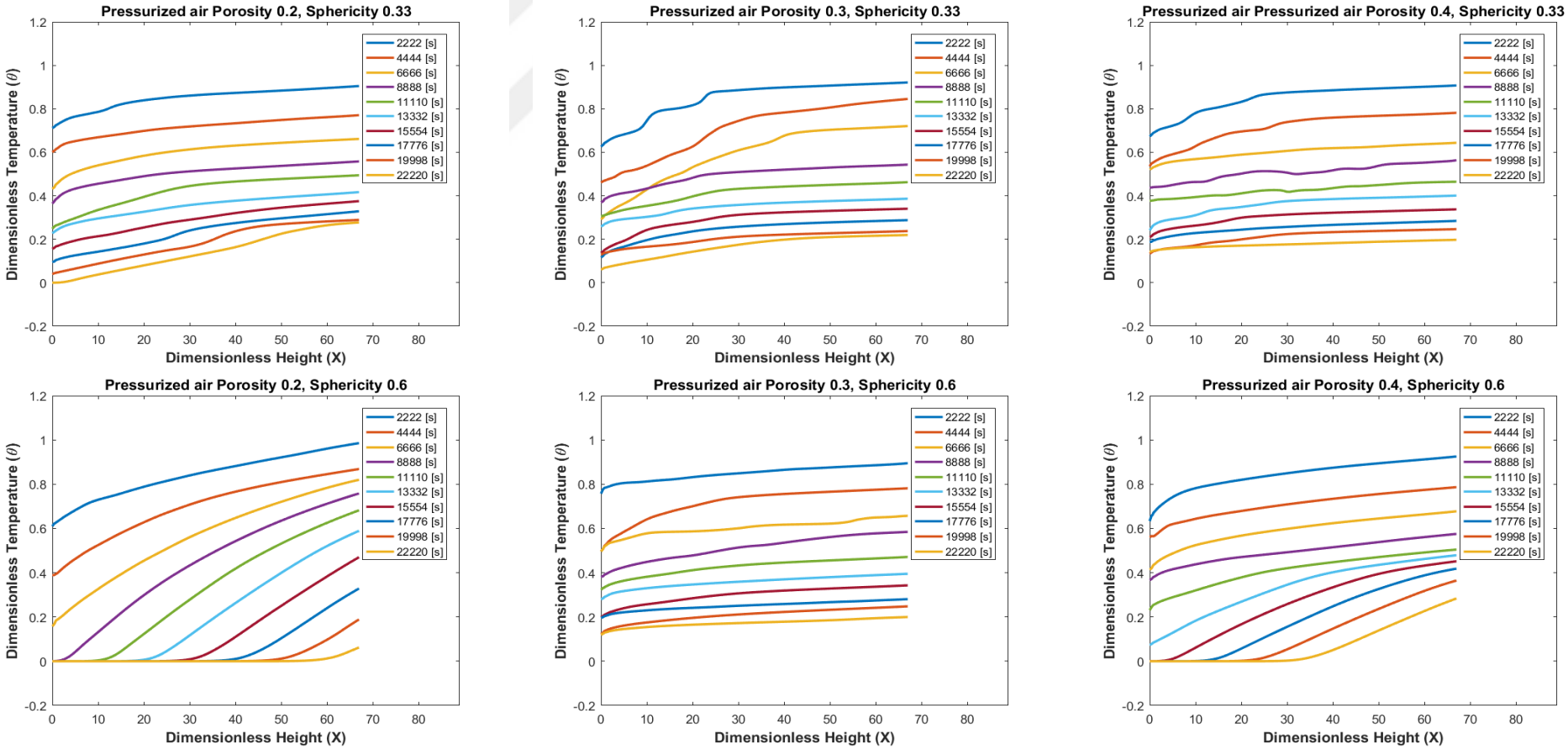

Figure B.1 : Axial variation of tank midline temperature during 6 hours of discharge for Pressurized Air (Part 1).

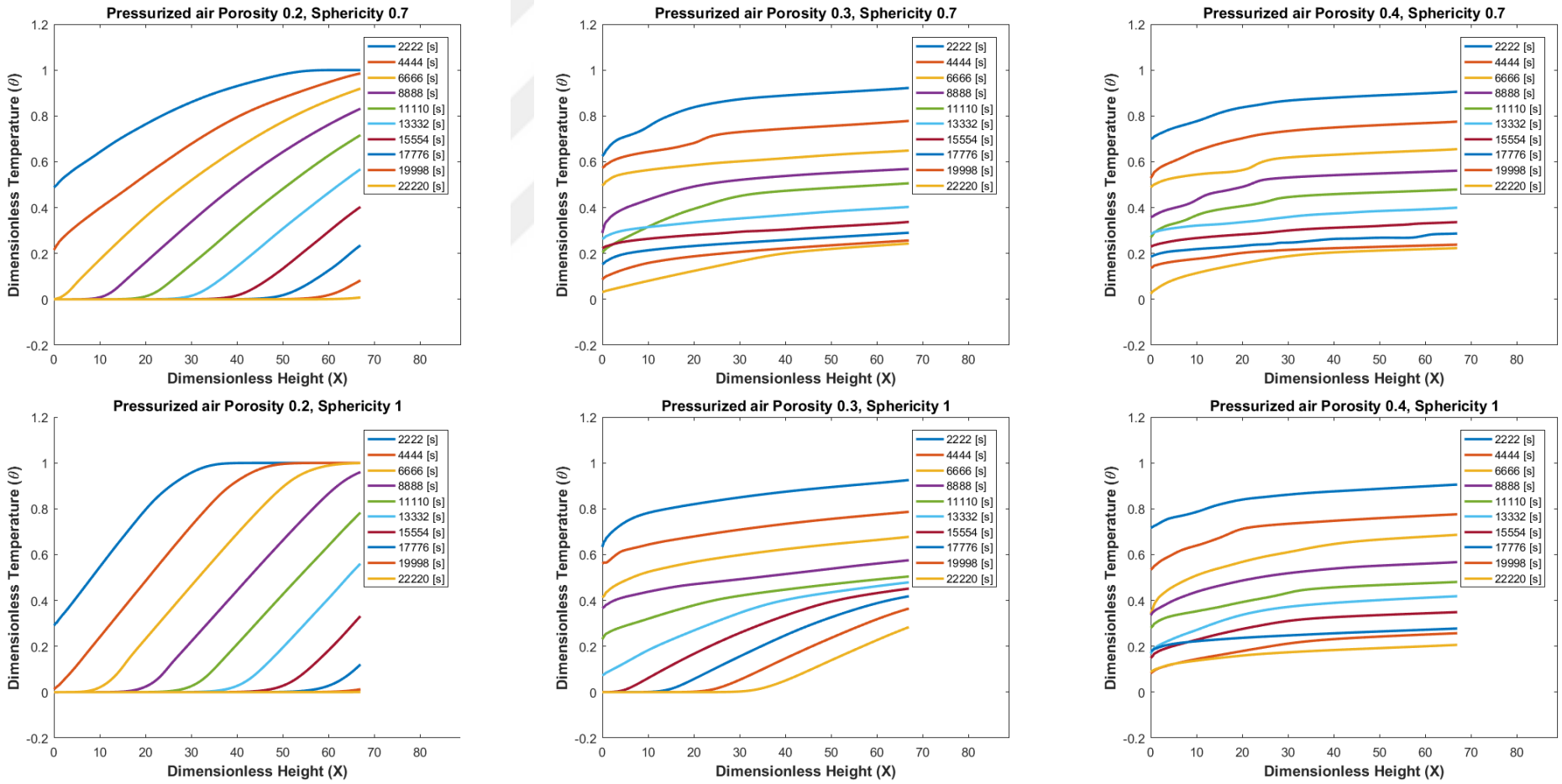

Figure B.2 : Axial variation of tank midline temperature during 6 hours of discharge for Pressurized Air (Part 2).

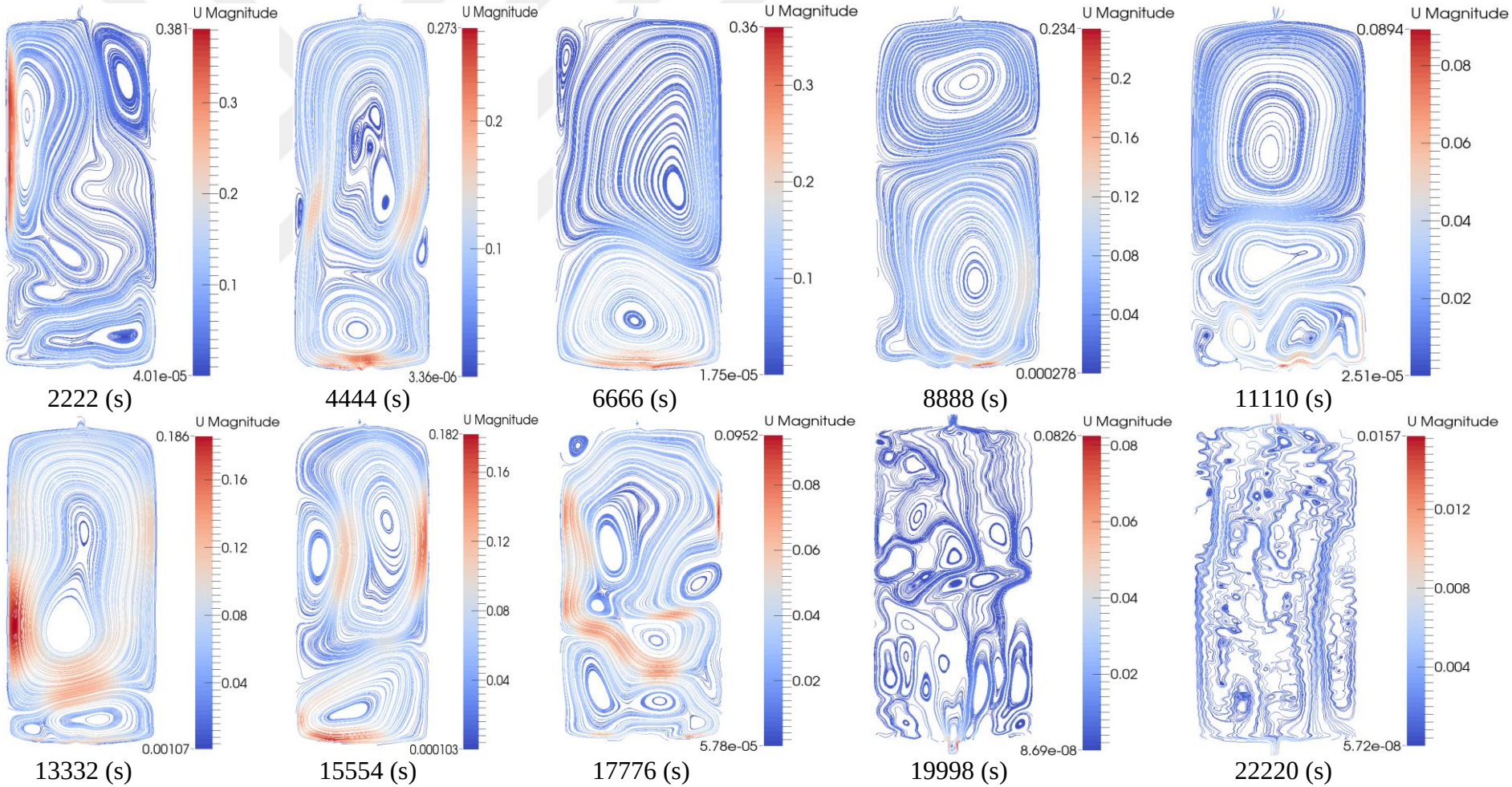

Figure B.3 : Variation of streamline of Pressurized Air during 6 hours of discharge for porosity 0.2 and sphericity 0.33 case.

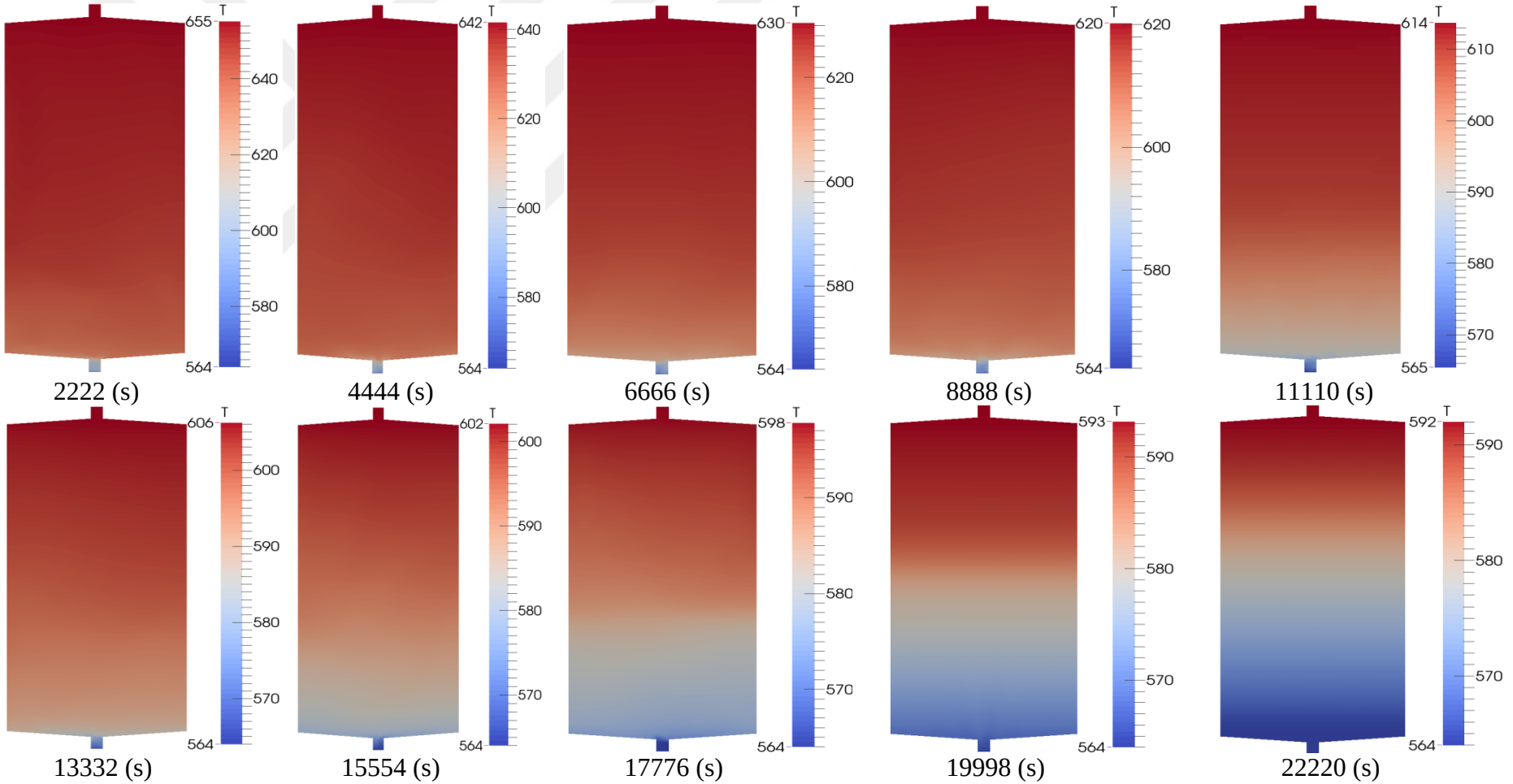

Figure B.4 : Variation of temperature profile of Pressurized Air during 6 hours of discharge for porosity 0.2 and sphericity 0.33 case.

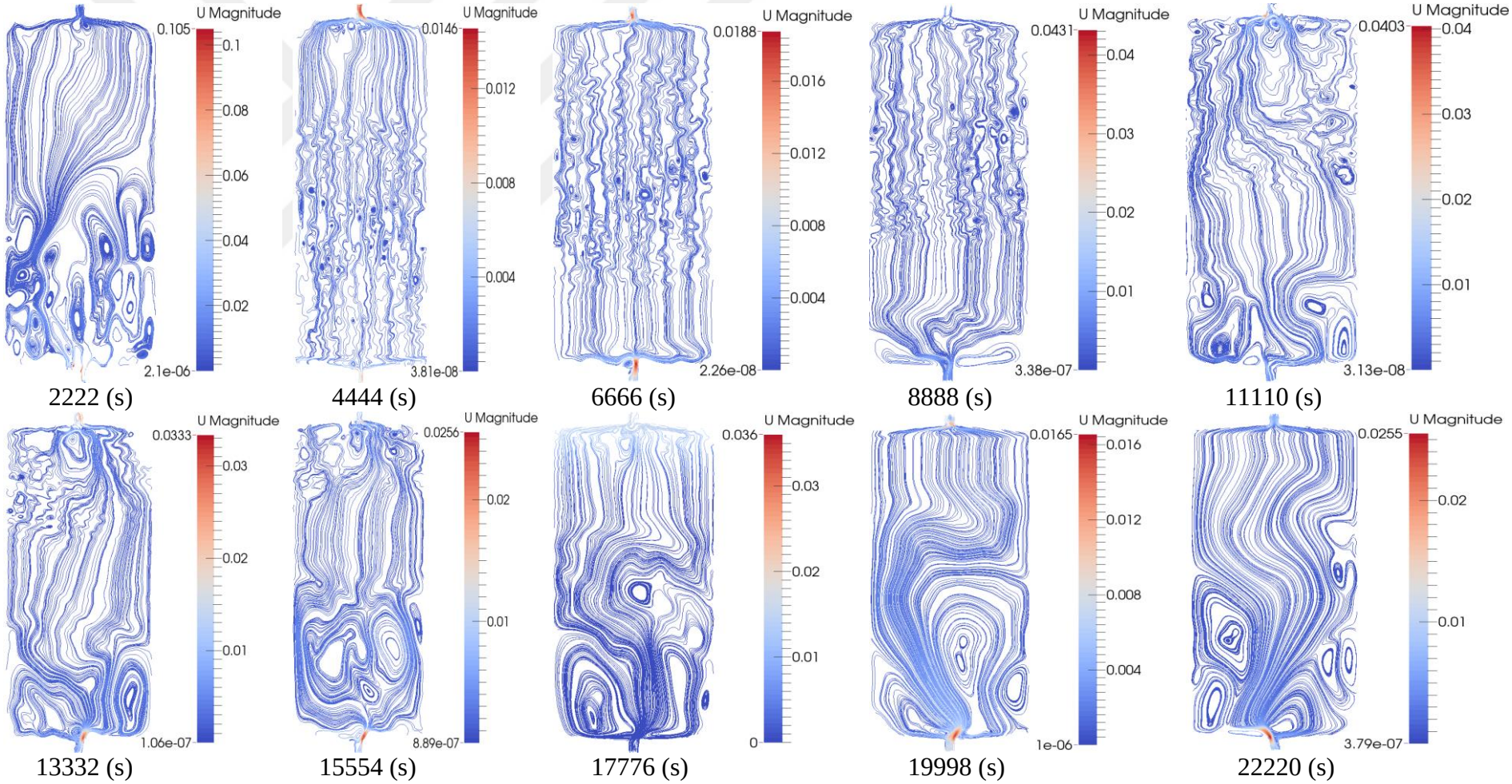

Figure B.5 : Variation of streamline of Pressurized Air during 6 hours of discharge for porosity 0.2 and sphericity 1 case.

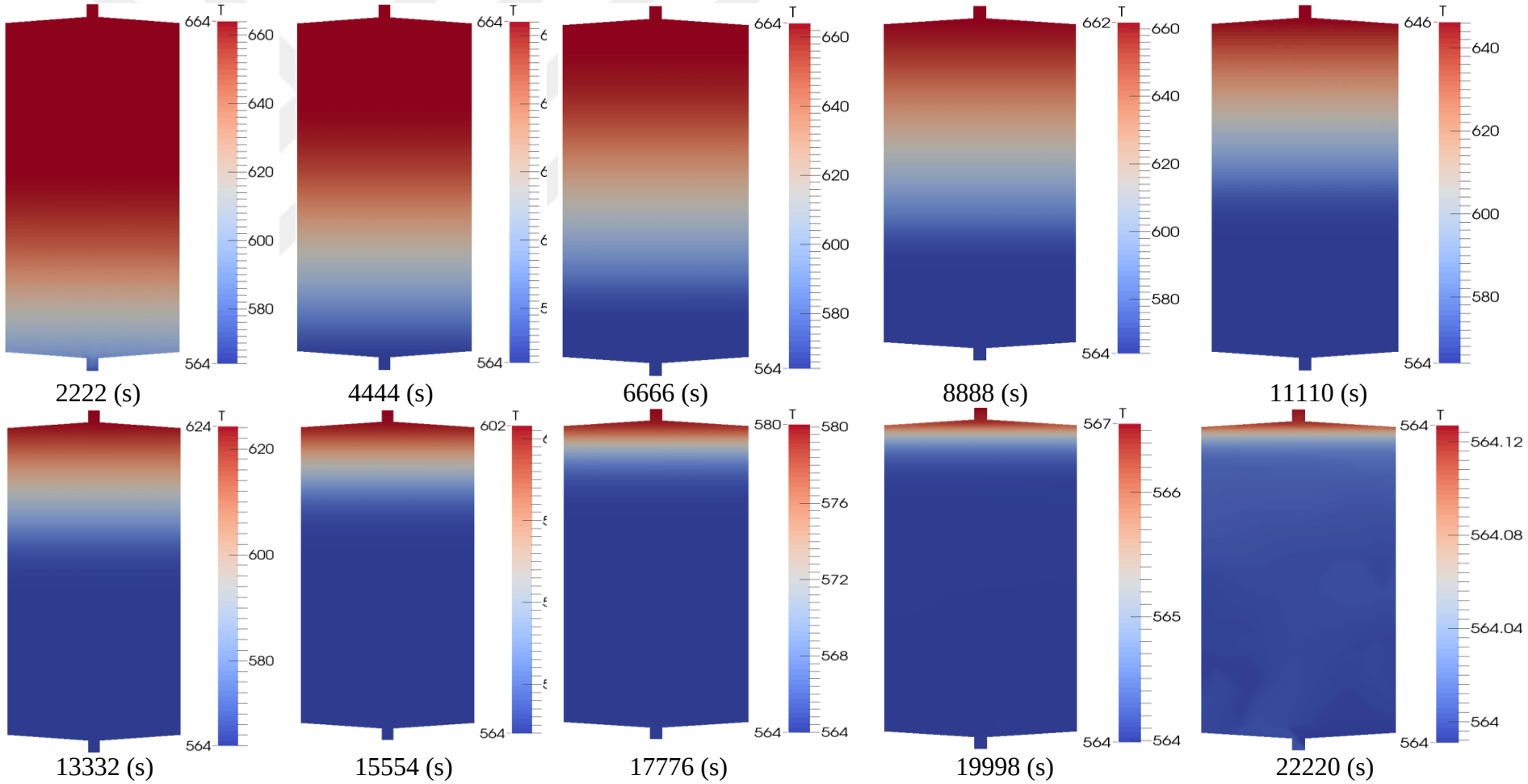

Figure B.6 : Variation of temperature profile of Pressurized Air during 6 hours of discharge for porosity 0.2 and sphericity 1 case.

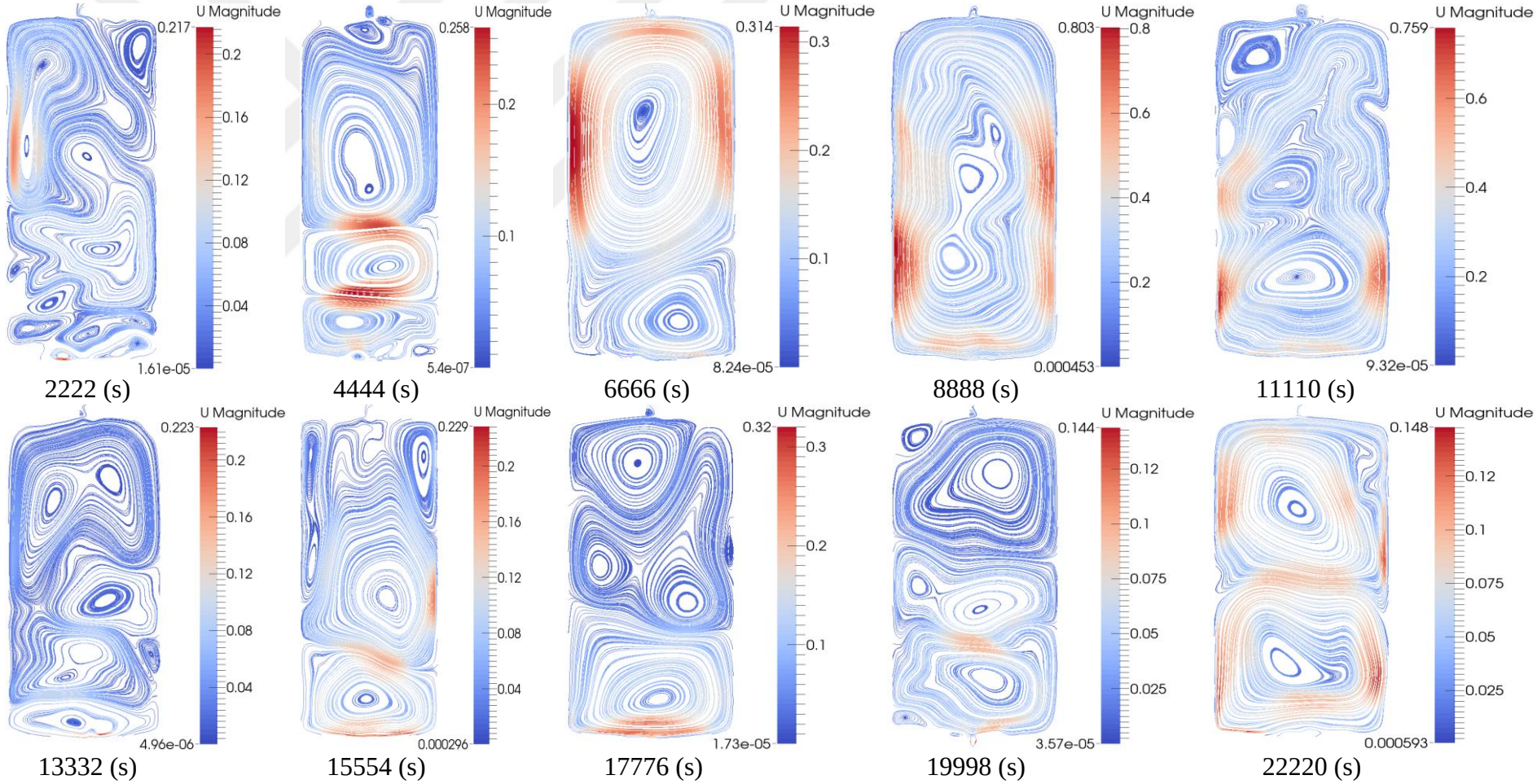

Figure B.7 : Variation of streamline of Pressurized Air during 6 hours of discharge for porosity 0.4 and sphericity 0.33 case.

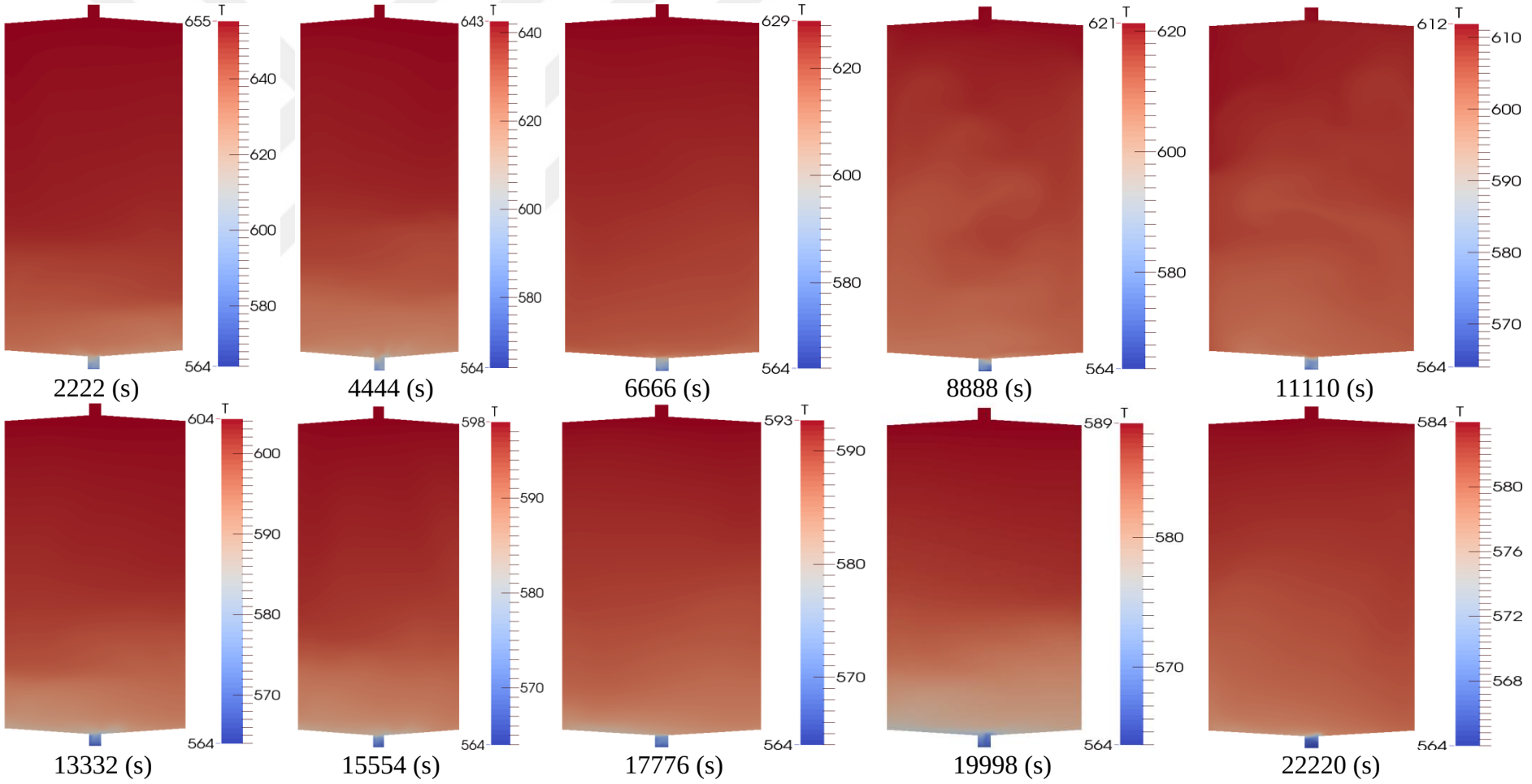

Figure B.8 : Variation of temperature profile of Pressurized Air during 6 hours of discharge for porosity 0.4 and sphericity 0.33 case.

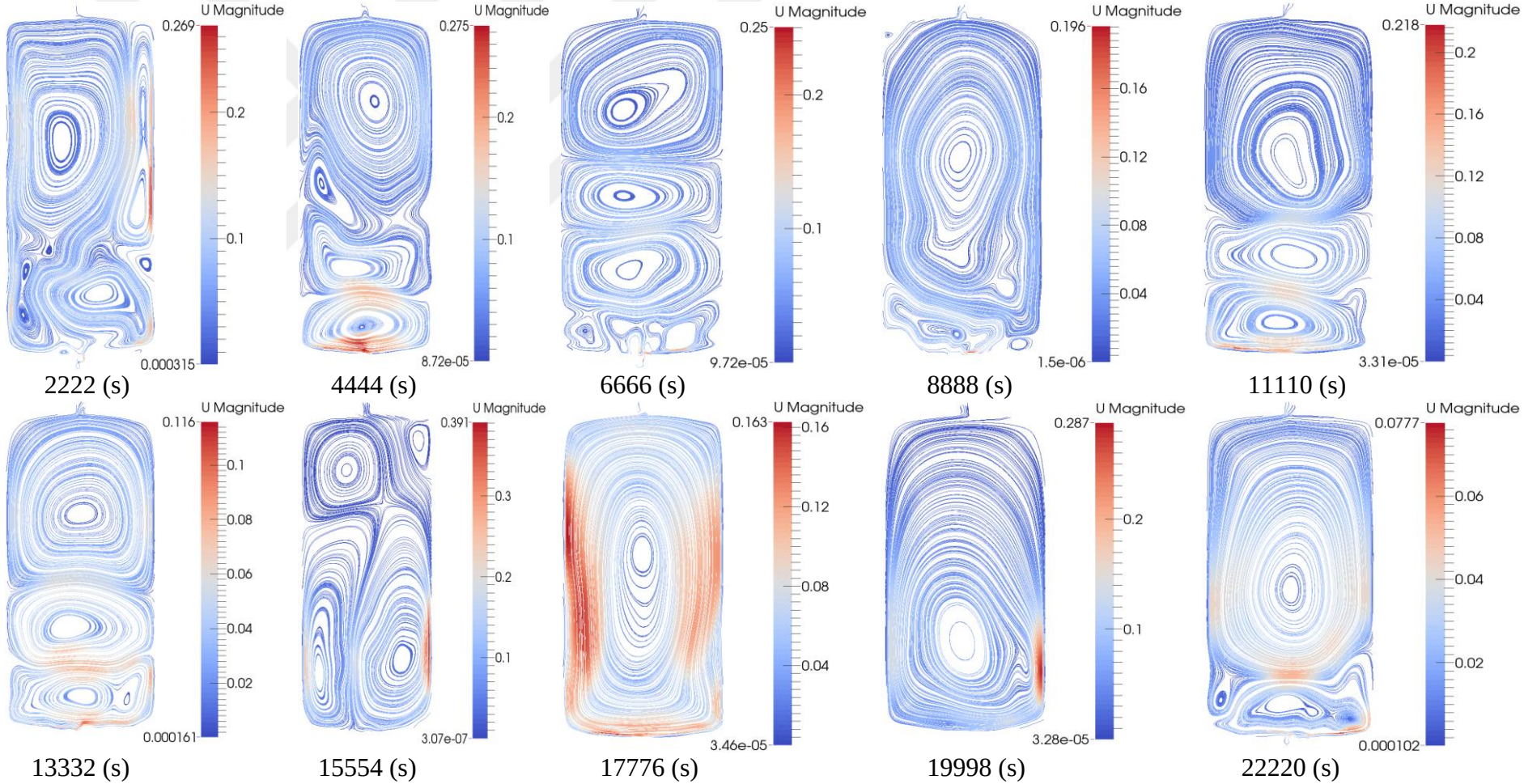

Figure B.9 : Variation of streamline of Pressurized Air during 6 hours of discharge for porosity 0.4 and sphericity 1 case.

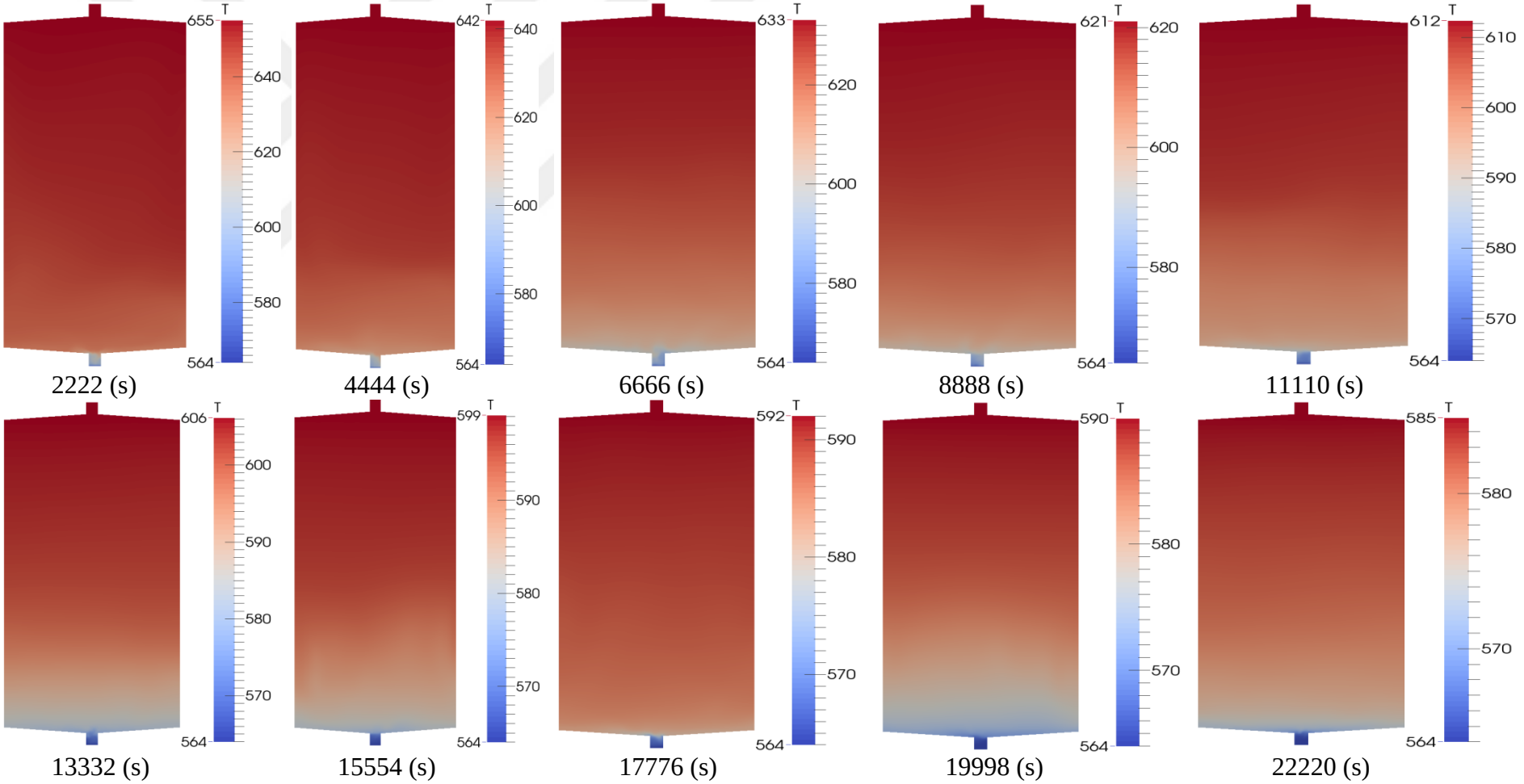

Figure B.10 : Variation of temperature profile of Pressurized Air during 6 hours of discharge for porosity 0.4 and sphericity 1 case.

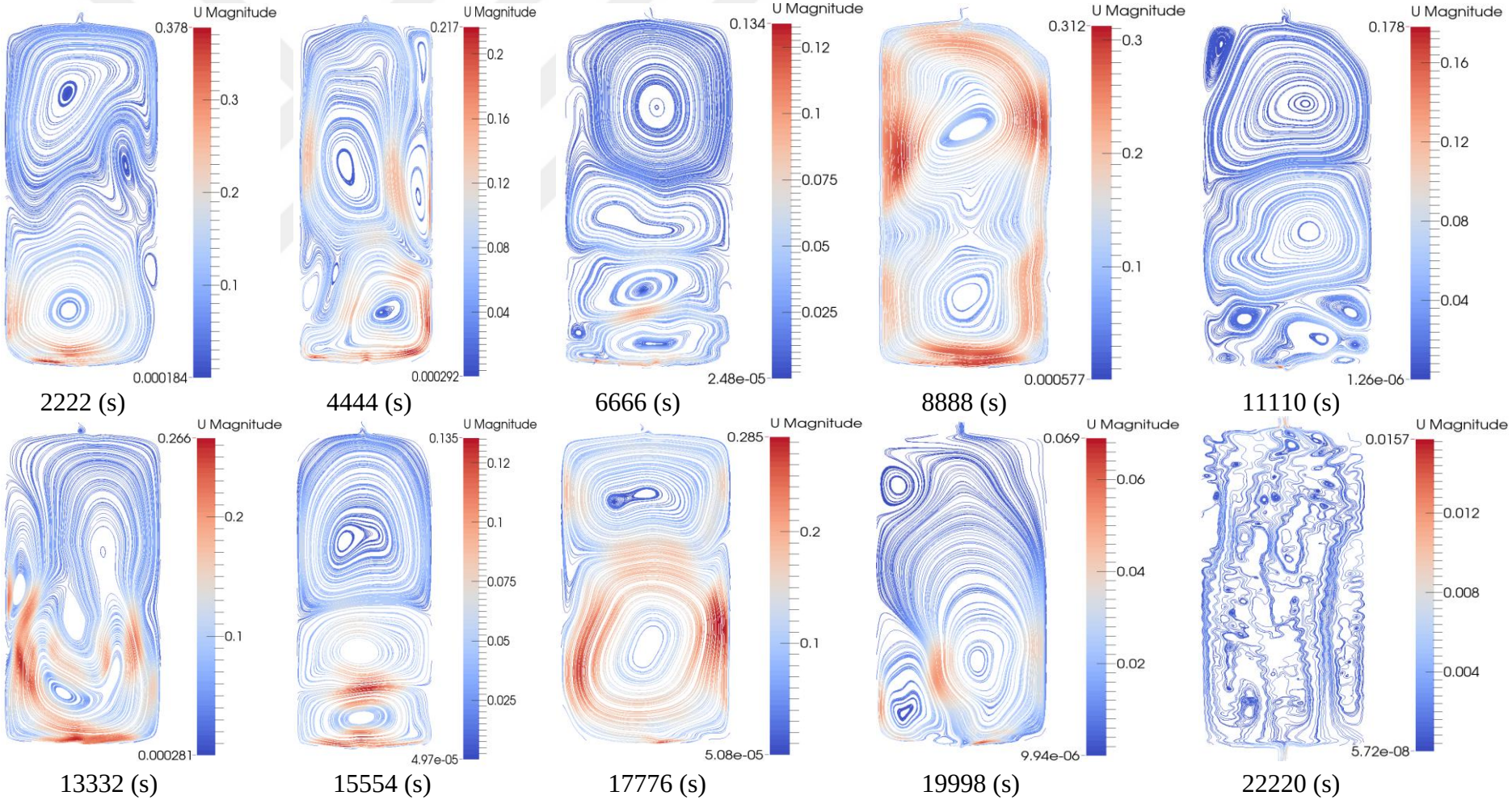

Figure B.11 : Variation of streamline of Solar Salt during 6 hours of discharge for porosity 0.2 and sphericity 0.33 case.

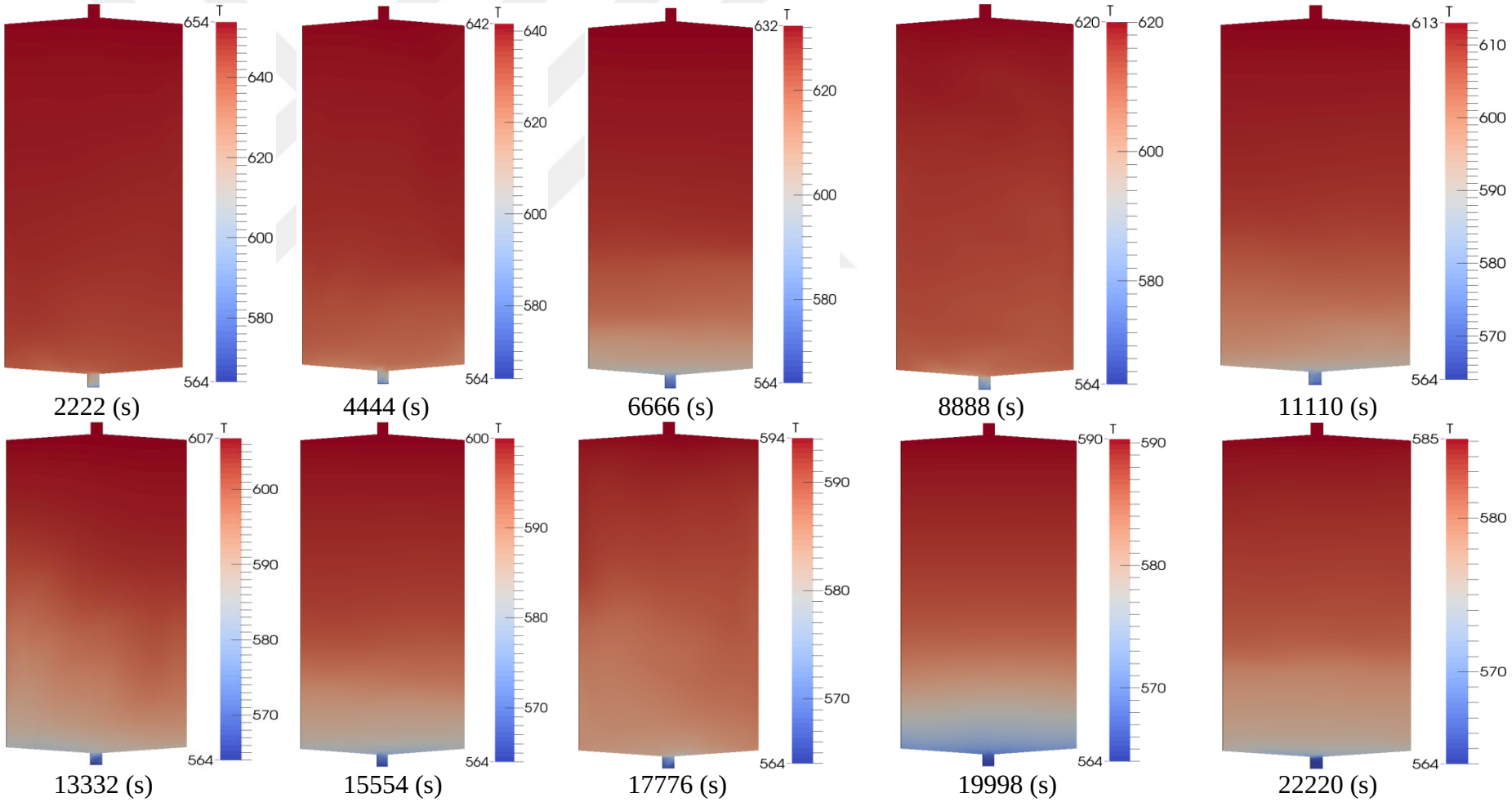

Figure B.12 : Variation of temperature profile of Solar Salt during 6 hours of discharge for porosity 0.2 and sphericity 0.33 case.

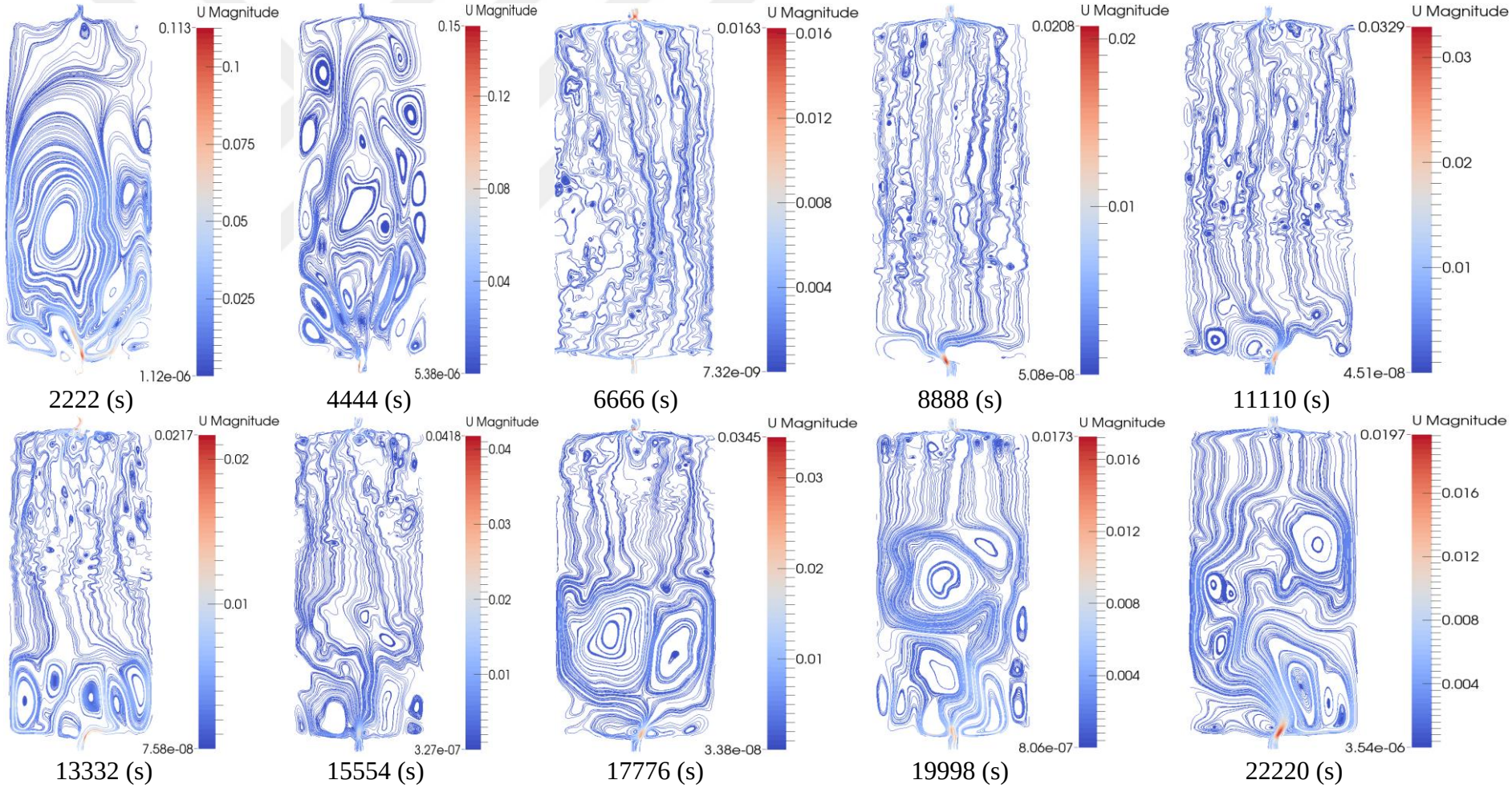

Figure B.13 : Variation of streamline of Solar Salt during 6 hours of discharge for porosity 0.2 and sphericity 1 case.

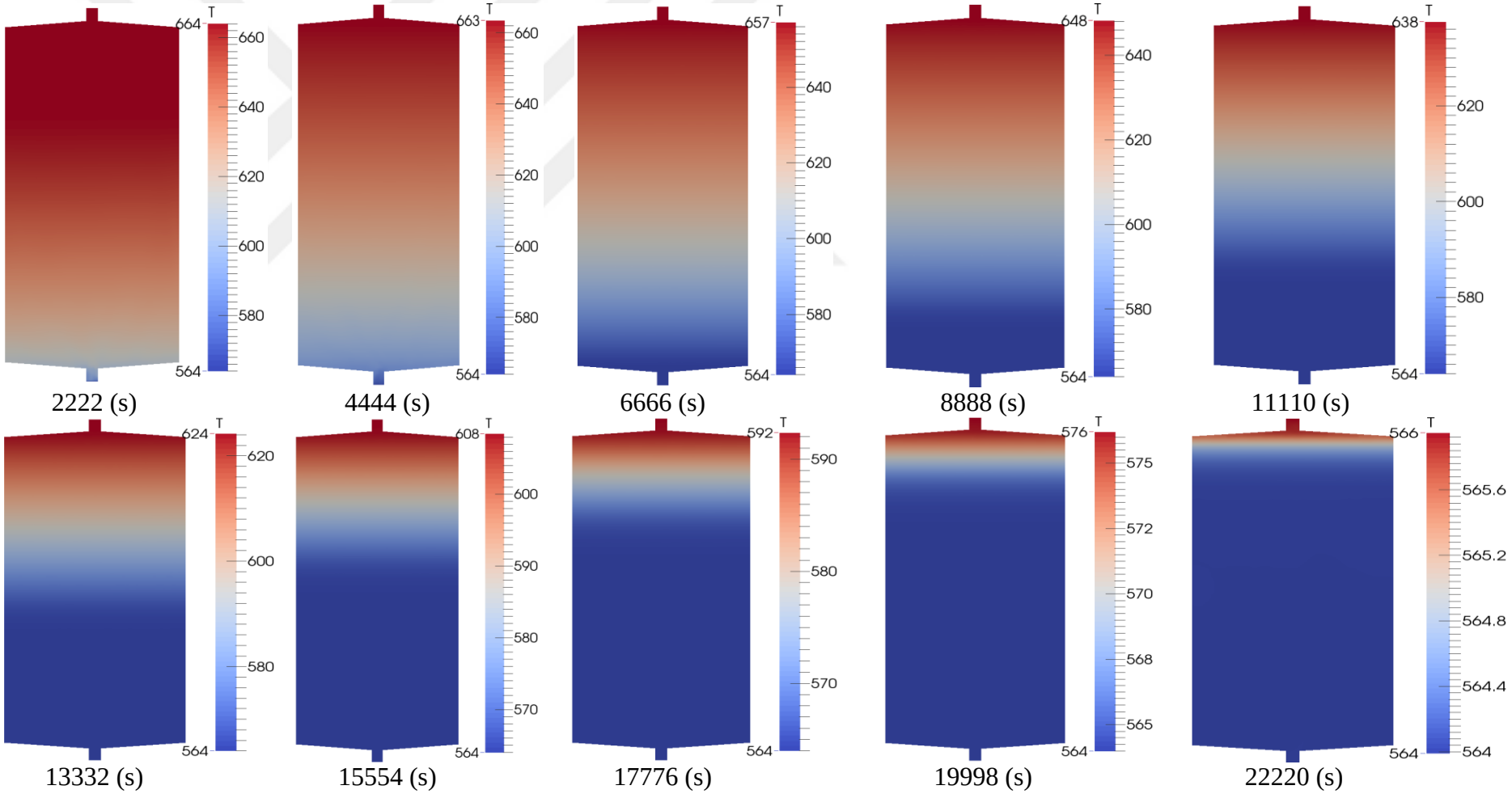

Figure B.14 : Variation of temperature profile of Solar Salt during 6 hours of discharge for porosity 0.2 and sphericity 1 case.

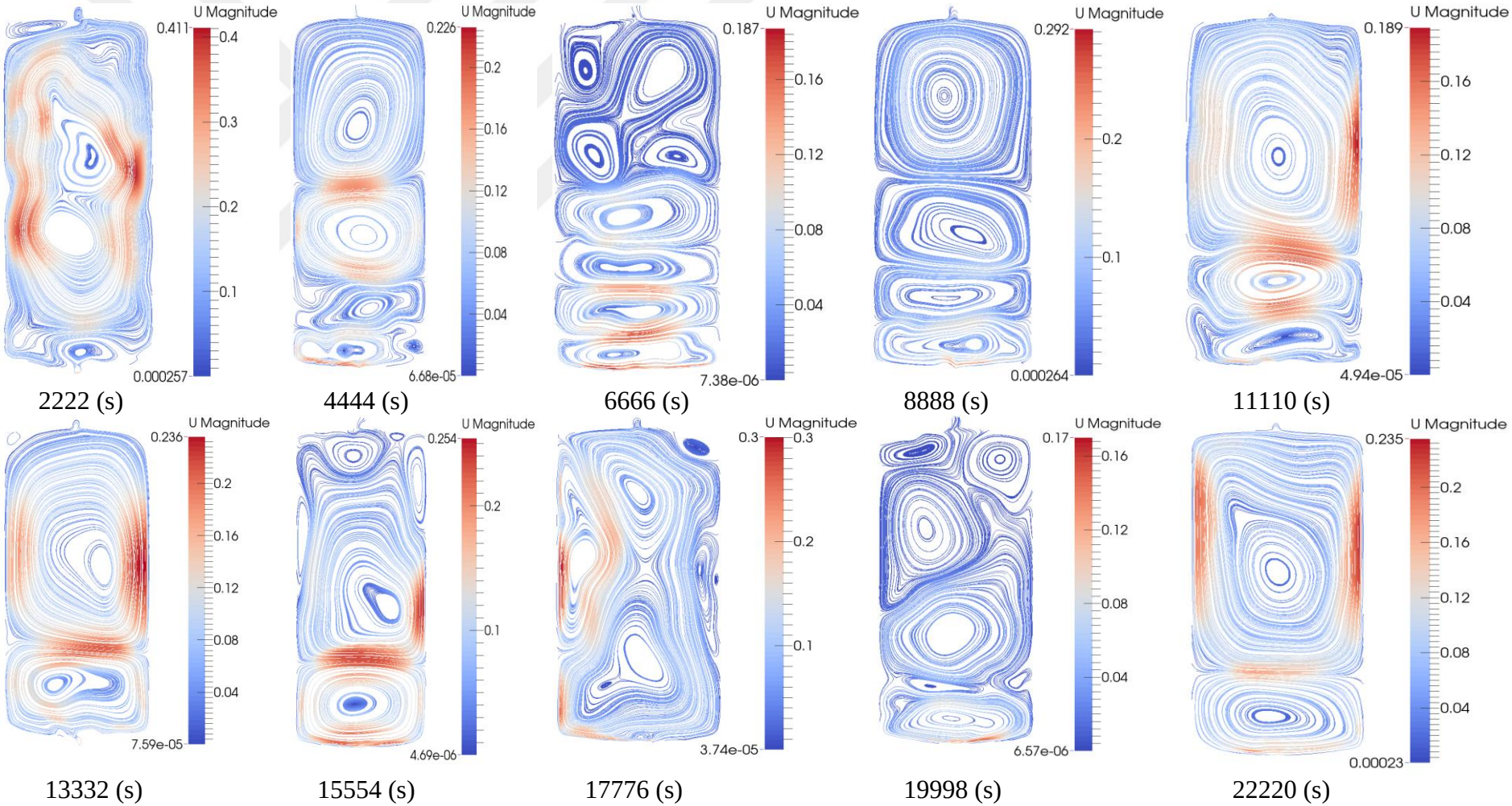

Figure B.15 : Variation of streamline of Solar Salt during 6 hours of discharge for porosity 0.4 and sphericity 0.33 case.

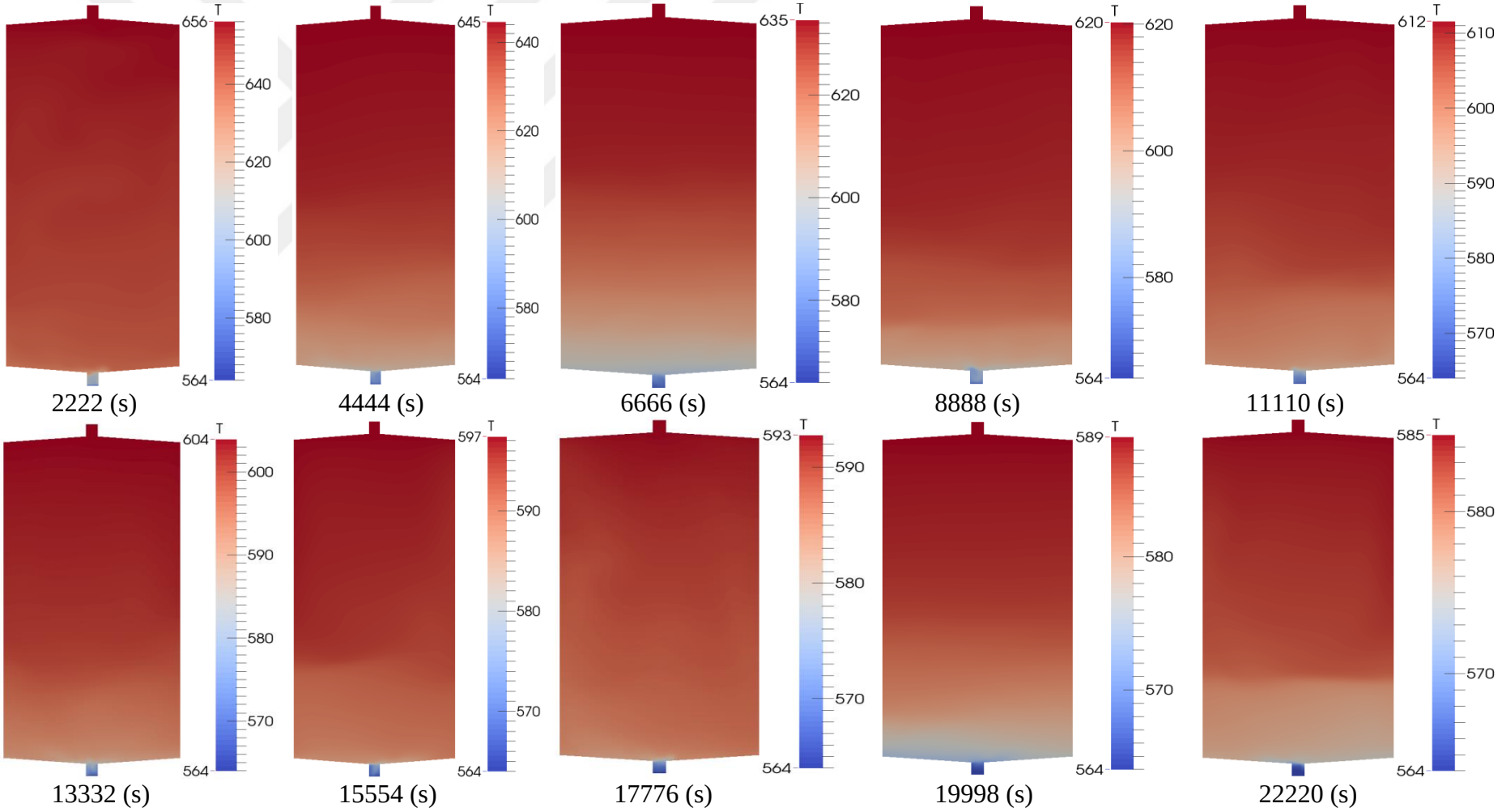

Figure B.16 : Variation of temperature profile of Solar Salt during 6 hours of discharge for porosity 0.4 and sphericity 0.33 case.

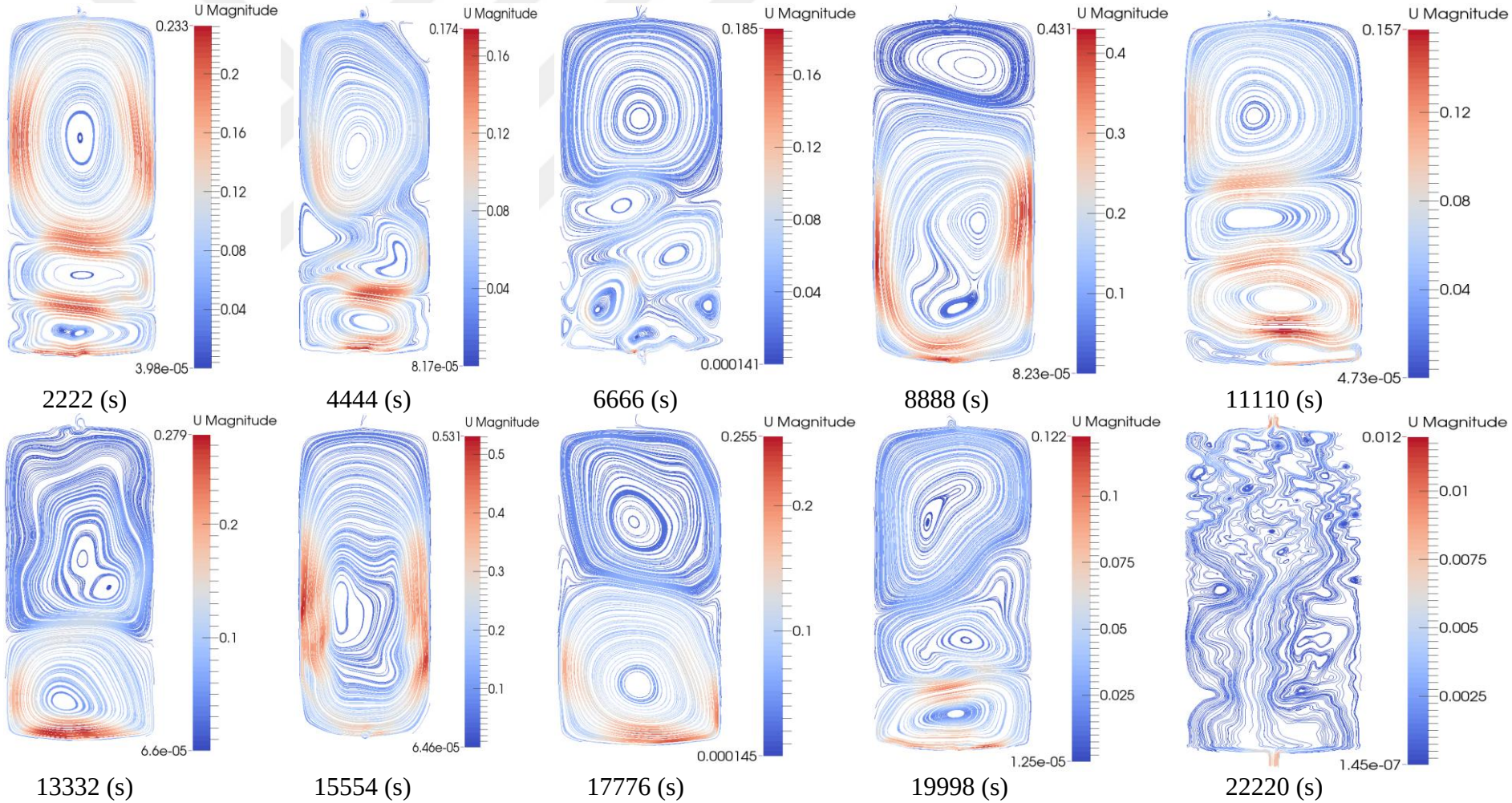

Figure B.17 : Variation of streamline of Solar Salt during 6 hours of discharge for porosity 0.4 and sphericity 1 case.

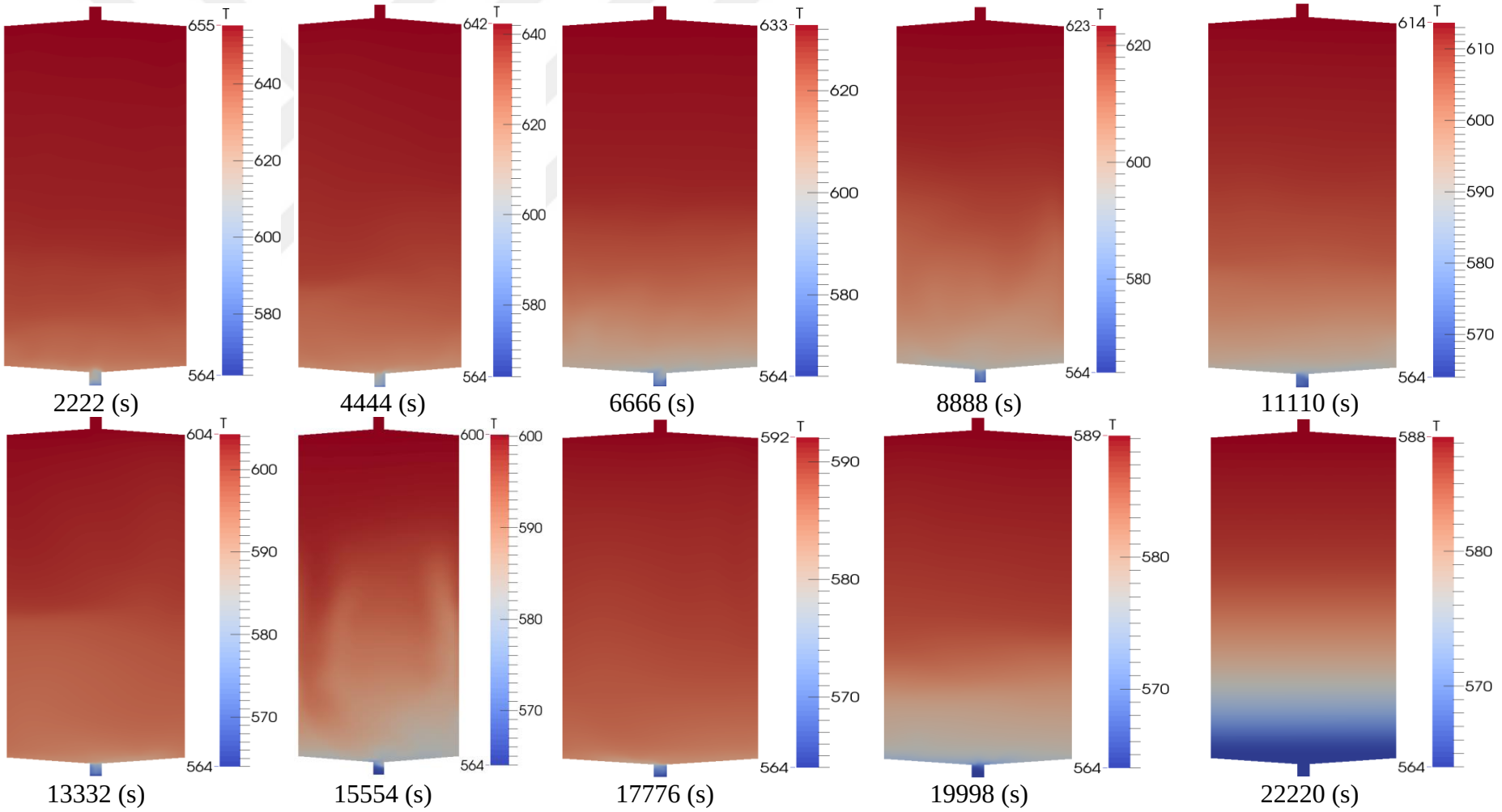

Figure B.18 : Variation of temperature profile of Solar Salt during 6 hours of discharge for porosity 0.4 and sphericity 1 case.

CURRICULUM VITAE

Name Surname: Azin Asaditaheri

E-Mail: Asaditaheri17@itu.edu.tr

EDUCATION:

B.Sc.: Mechanical Engineering

M.Sc.: Energy Science and Technology

PUBLICATIONS, PRESENTATIONS AND PATENTS ON THE THESIS:

OTHER PUBLICATIONS, PRESENTATIONS AND PATENTS:

- Taghizadeh S**, Asaditaheri A.** 2018: Heat transfer and entropy generation of laminar mixed convection in an inclined lid driven enclosure with a circular porous cylinder. *International Journal of Thermal Science*, 134, 242-257.

- Makouie N, **Asaditaheri A.** 2014: NUMERICAL INVESTIGATION OF BUBBLE GROWTH UNDER HEAT TRANSFER, *Indian Journal of Science Research*, 1, 275-279.

- **Asaditaheri A,** Mohammadi M, 2018: Bubble behavior in an ultrasonic field; stability analyses with bifurcation diagram: Effect of initial bubble radius, surrounding liquid viscosity and ultrasonic pressure. *International Conference On New Horizons in The Engineering Science*, August 9, 2018 Istanbul, Turkey.

- Mohammadi M, **Asaditaheri A,** Alizad F, Khalili Hezarjaribi M, 2016: Bubble Behavior in an Ultrasonic Field, Stability Analyses with Bifurcation Diagram: Effect of Polytrophic Gas Exponent, Hydrostatic Pressure and Ultrasonic Pressure. *4th International Conference On Engineering and Humanities*, September 17-18, 2016 Kiev, Ukraine.